

# Coordinated Sum-Rate Maximization in Multicell MU-MIMO with Deep Unrolling

Lukas Schynol, Marius Pesavento

**Abstract**—Coordinated weighted sum-rate maximization in multicell MIMO networks with intra- and intercell interference and local channel state at the base stations is recognized as an important yet difficult problem. A classical, locally optimal solution is obtained by the weighted minimum mean squared error (WMMSE) algorithm which facilitates a distributed implementation in multicell networks. However, it often suffers from slow convergence and therefore large communication overhead. To obtain more practical solutions, the unrolling/unfolding of traditional iterative algorithms gained significant attention. In this work, we demonstrate a complete unfolding of the WMMSE algorithm for transceiver design in multicell MU-MIMO interference channels with local channel state information. The resulting architecture termed GCN-WMMSE applies ideas from graph signal processing and is agnostic to different wireless network topologies, while exhibiting a low number of trainable parameters and high efficiency w.r.t. training data. It significantly reduces the number of required iterations while achieving performance similar to the WMMSE algorithm, alleviating the overhead in a distributed deployment. Additionally, we review previous architectures based on unrolling the WMMSE algorithm and compare them to GCN-WMMSE in their specific applicable domains.

**Index Terms**—Deep unrolling, deep unfolding, WMMSE algorithm, coordinated downlink beamforming, multiuser MIMO, multicell network, graph convolutional neural network.

## I. INTRODUCTION

Multiple-input multiple-output (MIMO) system theory has been instrumental in meeting the spectral efficiency and capacity targets of modern wireless systems [1]. When considering downlink beamforming with instantaneous channel state information (CSI), a common utility function to design optimal transmit and receive beamformers given transmit power limitations is the constrained weighted sum-rate (WSR) maximization. Treating interference as noise for simple receivers, the objective is multimodal and its optimization is NP-hard, even for the single-antenna case or a single-cell network [2], [3]. Globally optimal algorithms such as [4] were developed but consequently require exponential runtime. In the space of locally optimal algorithms, the weighted minimum mean squared error (WMMSE) iterative algorithm [5] is widely regarded as

a benchmark for WSR maximization due to the high sum-rate it attains while its updates can be expressed in closed-form. Furthermore, it is applicable in multicell systems and can be deployed in a distributed fashion with limited communication overhead per iteration, eliminating the necessity to collect the total channel state information at a central point. Depending on the channel conditions, the WMMSE algorithm requires a large number of iterations to converge. The authors of [6] proposed an algorithm based on fractional programming which converges in fewer iterations than the WMMSE algorithm. However, it adds significant complexity by introducing an additional convex subproblem per iteration which itself must be iteratively solved. Nevertheless, due to their associated runtime or communication overhead, optimization-based iterative solutions are difficult to apply in practice.

In recent years, machine learning methods have been identified as one of the key components for the design and operation of future communication networks [7]–[9]. Among other use cases such as resource management [10], detection [11] or channel estimation [12], the application of deep learning on transmit power allocation and downlink beamforming has been explored [13]–[17]. Particularly in beamforming, neural networks exhibit promising results w.r.t. their achieved sum-rate performance compared to their computational complexity.

First explicitly explored in [18], the concept of algorithm unfolding or algorithm unrolling recently gained significant interest in the signal processing community [19], [20]. While many state-of-the-art techniques incorporate components of classical algorithms into their corresponding deep network architecture, algorithm unrolling takes this notion further by viewing iterations of these problem-specific algorithms as layers of machine learning models. Given that the function representing the objective variable update in one iteration can be made fully differentiable, we can unfold a finite number of iterations, introduce new parameters and train them on data using established stochastic gradient descent (SGD) techniques. This way of combining expert knowledge with machine learning concepts can lead to better generalization performance and interpretability of unrolling-based architectures compared to conventional neural network architectures. These two factors are key for robust wireless communication networks, and together with the already existing body of algorithms based on rigorous optimization, algorithm unrolling is an attractive alternative to the use of generic network architectures.

Several works applied the concept of algorithm unrolling to the problem of downlink beamforming. In [21], efficient solutions to the WSR maximization in multiple-input single-output (MISO) networks consisting of transmitter-receiver

The authors acknowledge the financial support by the Federal Ministry of Education and Research of Germany in the project "Open6GHub" (grant no. 16KISK014). The computations for this research paper were conducted on the Lichtenberg high performance computer of the TU Darmstadt. This article was presented in part at the 30th European Signal Processing Conference (EUSIPCO), 2022.

Lukas Schynol (corresponding author) and Marius Pesavento are with the Communication Systems Group, Technische Universität Darmstadt, Darmstadt, Germany; Emails: {lschynol, pesavento}@nt.tu-darmstadt.de

Accepted for publication in IEEE Journal on Selected Areas in Communications.

pairs are found by unrolling the inexact cyclic coordinate descent method [22]. In [23], a substep of the WMMSE algorithm is replaced by a secondary projected gradient descent (PGD) optimization, the step sizes of which are learned using data, thereby facilitating a trade-off between performance and complexity. However, the discussion in [23] is limited to single-cell MISO networks. The architecture proposed in [24] approximates and unfolds matrix inversion operations within the updates of the WMMSE algorithm, achieving performance close to the WMMSE in the single-cell MIMO case with multiple users (MU). The authors of [25] consider a multicell scenario of pairwise single-input single-output (SISO) links and incorporate graph neural networks (GNNs) [26] into the WMMSE variable updates in order to reduce the number of required iterations.

In this paper, the structure of graph convolutional networks (GCNs) is applied to unfold the WMMSE algorithm in its most general form, i.e., coordinated multicell multi-user (MU)-MIMO networks. Unlike other approaches [15], [25], [27] based on GNNs, in which the graph underlying the GNN mimicks the wireless network topology, our GNN graph shift matrices represent transceiver signal spaces to achieve generality in the number of transceiver antennas. To our best knowledge, transceiver design algorithms based on deep unrolling have not yet been considered in general network scenarios including MU-MIMO cells with inter- and intracell interference. We set the following requirements and goals for our deep unfolded network:

- Compared to previous literature, we focus on a machine learning architecture that is at least as general as the original WMMSE algorithm, and that is robust to changing network configurations after training.
- The number of iterations must reduce while the computational effort per iteration must not exceed the complexity order of the original WMMSE algorithm.
- The communication overhead per iteration for distributed implementations must be equal or less compared to the WMMSE algorithm to capitalize on the reduced number of iterations.

Our contributions are:

- 1) Utilizing GCNs as spatial signal filters, we propose a completely general unfolding architecture of the WMMSE algorithm for WSR maximization in multicell MU-MIMO networks that meets the above requirements, which we denote as GCN-WMMSE.
- 2) We propose an accelerated dual variable update procedure based on rational function approximation for the classical WMMSE algorithm and the forward pass of our GCN-WMMSE networks. In the backward pass, we provide an efficient network parameter update scheme based on the notion of implicit functions. Furthermore, we pinpoint numerical issues that can arise for both methods.
- 3) We demonstrate the excellent generalization capability and training data efficiency of the proposed GCN-WMMSE architecture in extensive simulations on Rayleigh fading and ray-tracing channel models. The resulting flexibility is exploited to reduce the cost of

communication and computation of model training.

- 4) We draw extensive comparisons to previously published unfolding methods, and extend their results by further experiments, leading to insights useful for future designs.

The rest of the paper is structured as follows: Section II defines the wireless system model and formulates the resource allocation problem, followed by a review of the WMMSE algorithm. The GCN-WMMSE architecture is proposed and motivated in Section III. Section IV presents the simulations results. In Section V, we relate our proposed architecture to previous works on WMMSE algorithm unrolling and provide additional simulation results with numerical comparisons. Section VI provides concluding remarks.

*Notation:* Uppercase  $\mathbf{X}$  and lowercase  $\mathbf{x}$  bold letters denote matrices and vectors respectively, where matrix elements are accessed by  $[\mathbf{X}]_{ij}$ .  $(\cdot)^H, (\cdot)^T, (\cdot)^{-1}$  and  $(\cdot)^\dagger$  denote the Hermitian transpose, transpose, inverse and Moore-Penrose inverse respectively. We denote the trace by  $\text{Tr}\{\cdot\}$ , the Frobenius norm by  $\|\cdot\|_F$  and the log-determinant w.r.t. the natural basis as  $\log\det(\cdot)$ .  $\mathbf{I}$  is the identity matrix,  $\mathbf{1}$  denotes a vector filled with ones.  $\nabla_{\mathbf{x}}$  denotes the gradient w.r.t. to some  $\mathbf{x}$ .  $f'$  denotes the derivative of a function  $f$  respectively.

## II. WEIGHTED MMSE MINIMIZATION

### A. System Model and Downlink Problem Formulation

Consider a wireless cellular system consisting of  $K$  cells, each of which are defined by a base station (BS). BS  $k$  is serving one of  $K$  disjoint subsets  $\{\mathcal{I}_k\}_{k=1}^K$  of users or user equipments (UEs), for a total of  $I = \sum_{k=1}^K |\mathcal{I}_k|$  UEs, and is equipped with an antenna array of size  $M_k$ , whereas every UE  $i$  is equipped with an array of  $N_i$  antennas. The output signal of the antenna array of BS  $k$  is modeled as the sum of mapped symbols  $\mathbf{x}_{\text{Tx},k} = \sum_{i \in \mathcal{I}_k} \mathbf{V}_i \check{\mathbf{s}}_i$  for  $k = 1, \dots, K$  where  $\mathbf{V}_i \in \mathbb{C}^{M_k \times N_i}$  is the complex downlink precoding matrix and  $\check{\mathbf{s}}_i \in \mathbb{C}^{N_i}$  with  $\mathbb{E}[\check{\mathbf{s}}_i \check{\mathbf{s}}_i^H] = \mathbf{I}$  is the symbol vector directed at UE  $i$  respectively<sup>1</sup>. We assume that the transceivers employ Gaussian code books and that the symbols are statistically independent between UEs. Given complex frequency-flat channel matrices  $\mathbf{H}_{ik} \in \mathbb{C}^{N_i \times M_k}$  from BS  $k$  to UE  $i$  and block-fading, the received signal of a user  $i$  assigned to BS  $k$  becomes

$$\mathbf{y}_{\text{Rx},i} = \mathbf{H}_{ik} \mathbf{V}_i \check{\mathbf{s}}_i + \sum_{m=1}^K \sum_{j \in \mathcal{I}_m \setminus \{i\}} \mathbf{H}_{im} \mathbf{V}_j \check{\mathbf{s}}_j + \mathbf{n}_i,$$

where  $\mathbf{n}_i \sim \mathcal{CN}(0, \sigma_i^2 \mathbf{I})$  is additive complex white Gaussian noise with power  $\sigma_i^2$  per antenna element. The second term both contains the intracell and intercell interference. We treat interference as noise at the UEs, thus, the achievable rate at UE  $i$  can be determined as  $\mathcal{R}_i = B \log\det(\mathbf{I} + \mathbf{Q}_i \mathbf{Z}_i^{-1})$  with  $\mathbf{Q}_i = \mathbf{H}_{ik} \mathbf{V}_i \mathbf{V}_i^H \mathbf{H}_{ik}^H$  being the covariance matrix of the useful signal and  $\mathbf{Z}_i = \sum_{m=1}^K \sum_{j \in \mathcal{I}_m \setminus \{i\}} \mathbf{H}_{im} \mathbf{V}_j \mathbf{V}_j^H \mathbf{H}_{im}^H + \sigma_i^2 \mathbf{I}$  being the covariance matrix of the interference plus noise. Without loss of generality the bandwidth  $B$  is set to unity.

The total WSR is given by  $\mathcal{R}_\Sigma = \sum_{i=1}^I \alpha_i \mathcal{R}_i$ , where  $\alpha_i > 0$  are predefined weights. Hence, the problem of maximizing

<sup>1</sup>Without loss of generality the number of data symbols per time instant per UE  $i$  is assumed to be equal to the number of receive antennas  $N_i$ .

the WSR under maximum power constraints can be formulated as

$$\begin{aligned} & \max_{\{\mathbf{V}_i\}_{i=1}^I} \sum_{i=1}^I \alpha_i \log \det (\mathbf{I} + \mathbf{Q}_i \mathbf{Z}_i^{-1}) \\ & \text{subject to } \sum_{i \in \mathcal{I}_k} \|\mathbf{V}_i\|_F^2 \leq P_k, \forall k \in \{1, \dots, K\}, \end{aligned} \quad (1)$$

where  $P_k$  for  $k = 1, \dots, K$  are the BS power budgets. In general, the objective function is highly multimodal, making a good optimum generally difficult to find [2], [3]. It must be remarked that although the above channel model is common in literature, the frequency flatness and instantaneous rate assumption are simplifications.

### B. WMMSE Algorithm

The authors of [5] tackle problem (1) by reformulating it to the WMMSE minimization

$$\begin{aligned} & \min_{\{\mathbf{U}_i, \mathbf{W}_i, \mathbf{V}_i\}_{i=1}^I} \sum_{i=1}^I \alpha_i (\text{Tr} \{\mathbf{W}_i \mathbf{E}_i\} - \log \det (\mathbf{W}_i)) \\ & \text{subject to } \sum_{i \in \mathcal{I}_k} \|\mathbf{V}_i\|_F^2 \leq P_k, \forall k \in \{1, \dots, K\} \\ & \quad \mathbf{W}_i \succeq \mathbf{0}, \forall i \in \{1, \dots, I\}, \end{aligned} \quad (2)$$

where  $\mathbf{E}_i = \mathbb{E} [(\tilde{\mathbf{s}}_i - \mathbf{U}_i^H \mathbf{y}_{\text{Rx},i})(\tilde{\mathbf{s}}_i - \mathbf{U}_i^H \mathbf{y}_{\text{Rx},i})^H]$  is the error covariance of the estimated symbol vector using the linear receive beamformer  $\mathbf{U}_i \in \mathbb{C}^{N_i \times N_i}$  and  $\mathbf{W}_i$  is the positive semidefinite (PSD) weight matrix assigned to UE  $i$ . Problem (1) and (2) share the optimal point and their stationary points. In a slight abuse of notations,  $\mathbf{U}$ ,  $\mathbf{W}$  and  $\mathbf{V}$  are defined as short hand for their respective set of receive beamformers  $\{\mathbf{U}_i\}_{i=1}^I$ , weight matrices  $\{\mathbf{W}_i\}_{i=1}^I$  and downlink beamformers  $\{\mathbf{V}_i\}_{i=1}^I$ . It is straightforward to show that the WMMSE objective in (2) is convex w.r.t.  $\mathbf{U}$ ,  $\mathbf{W}$  and  $\mathbf{V}$  individually. By subsequently deriving their first-order stationary points, the block coordinate descent (BCD) algorithm [28] with updates

$$(\mathbf{U}\text{-Step}) \quad \forall i : \mathbf{U}_i^{(\ell)} = (\mathbf{J}_i^{(\ell)})^{-1} \mathbf{H}_{ik} \mathbf{V}_i^{(\ell-1)} \quad (3a)$$

$$(\mathbf{W}\text{-Step}) \quad \forall i : \mathbf{W}_i^{(\ell)} = \left( \mathbf{I} - (\mathbf{V}_i^{(\ell-1)})^H \mathbf{H}_{ik}^H \mathbf{U}_i^{(\ell)} \right)^{-1} \quad (3b)$$

$$\begin{aligned} (\mu\text{-Step}) \quad \forall k : \mu_k^{(\ell)} &= \underset{\mu_k}{\text{argmax}} \mu_k \\ & \text{subject to } 0 = f_{\text{CS},k}^{(\ell)}(\mu_k), \mu_k \geq 0, \end{aligned} \quad (3c)$$

$$(\mathbf{V}\text{-Step}) \quad \forall i : \mathbf{V}_i^{(\ell)} = \left( \mathbf{R}_k^{(\ell)} + \mu_k^{(\ell)} \mathbf{I} \right)^\dagger \tilde{\mathbf{V}}_i^{(\ell)} \quad (3d)$$

is obtained [5]. Note that the indices  $k$  and  $i$  are chosen such that  $i \in \mathcal{I}_k$  throughout. The updates are performed sequentially. Here we defined  $\mathbf{J}_i^{(\ell)} = \sum_{m=1}^K \sum_{j \in \mathcal{I}_m} \mathbf{H}_{im} \mathbf{V}_j^{(\ell-1)} (\mathbf{V}_j^{(\ell-1)})^H \mathbf{H}_{im}^H + \sigma_i^2 \mathbf{I}$  as the receive signal covariance matrix at UE  $i$ ,

$$\mathbf{R}_k^{(\ell)} = \sum_{j=1}^I \alpha_j \mathbf{H}_{jk}^H \mathbf{U}_j^{(\ell)} \mathbf{W}_j^{(\ell)} (\mathbf{U}_j^{(\ell)})^H \mathbf{H}_{jk} \quad (4)$$

as the weighted uplink covariance matrix at BS  $k$  and

$$\tilde{\mathbf{V}}_i^{(\ell)} = \alpha_i \mathbf{H}_{ik}^H \mathbf{U}_i^{(\ell)} \mathbf{W}_i^{(\ell)} \quad (5)$$

as the candidate beamformer matrix of UE  $i \in \mathcal{I}_k$  at BS  $k$  respectively. Note that  $\mathbf{W}_i$  in (3b) is merely the inverse of the resulting minimum mean squared error (MMSE) covariance matrix  $\mathbf{E}_i^{\text{MMSE}}$  at the receiver. Equations (3c) and (3d) result

from applying Karush-Kuhn-Tucker (KKT) conditions to solve for  $\mathbf{V}_i^{(\ell)}$  under the constraint  $\sum_{i \in \mathcal{I}_k} \|\mathbf{V}_i^{(\ell)}\|_F^2 \leq P_k$ , thereby introducing dual variables  $\mu_k^{(\ell)}$  for  $k = 1, \dots, K$  at iteration  $\ell$ , as well as the complementary slackness condition  $f_{\text{CS},k}^{(\ell)}(\mu_k) = 0$  where

$$f_{\text{CS},k}^{(\ell)}(\mu_k) = \left( v_k^{(\ell)}(\mu_k) - 1 \right) \mu_k \quad (6)$$

$$\text{and } v_k^{(\ell)}(\mu_k) = \sum_{m=1}^{M_k} \frac{\varphi_{km}^{(\ell)}}{(\lambda_{km}^{(\ell)} + \mu_k)^2}. \quad (7)$$

The quantities  $\lambda_{km}^{(\ell)} = [\Lambda_k^{(\ell)}]_{mm}$  and  $\varphi_{km}^{(\ell)} = [\Phi_k^{(\ell)}]_{mm}$  are obtained from the eigendecomposition of the normal matrix  $\mathbf{R}_k^{(\ell)} = \mathbf{D}_k^{(\ell)} \Lambda_k^{(\ell)} (\mathbf{D}_k^{(\ell)})^H$  and  $\Phi_k^{(\ell)} = \frac{1}{P_k} (\mathbf{D}_k^{(\ell)})^H \left( \sum_{i \in \mathcal{I}_k} \tilde{\mathbf{V}}_i^{(\ell)} (\tilde{\mathbf{V}}_i^{(\ell)})^H \right) \mathbf{D}_k^{(\ell)}$ , respectively. To satisfy the complementary slackness condition (6), the authors of [5] propose the bisection search to find the root of  $v_k(\mu_k) - 1 = 0$ . Shi et al. establish convergence of the WMMSE algorithm to a stationary point. It is critical to remark that, compared to [5], we apply the Moore-Penrose inverse in (3d) instead of the standard inverse. Update (3d) is the *exact* minimizer of the block variable and covers particular occurring instances in which the matrix  $\mathbf{R}_k^{(\ell)} + \mu_k^{(\ell)} \mathbf{I}$  proves to be singular and the original update rule does not apply.

Importantly, the algorithm can be implemented in a distributed fashion by computing  $\mathbf{U}$ -updates and  $\mathbf{W}$ -updates at the respective UEs and each BS computes  $\mathbf{V}$  only for its assigned beamformers. Each UE needs to locally estimate  $\mathbf{J}_i$  and requires information about their assigned precoding matrix as well as the channel toward its assigned BS. The BSs on the other hand require local CSI, the matrix  $\mathbf{U}_i \mathbf{W}_i \mathbf{U}_i^H$  for each UE within their cell radius as well as the matrix  $\mathbf{U}_i \mathbf{W}_i$  of their assigned UEs.

### III. PROPOSED WMMSE UNFOLDING ARCHITECTURE

In this section, we introduce the proposed Graph-Convolutional-Network-WMMSE architecture, or GCN-WMMSE in short. First, in Section III-A, we review the concept of unfolding and define a neural network based on the general WMMSE as our starting point. In Section III-B, the GCN-WMMSE architecture is obtained by unfolding the baseline WMMSE algorithm. It aims to reduce the required number of iterations, leading to a lower computational cost and overhead in distributed deployments. Section III-C details the training procedure that will be used to learn the parameters of GCN-WMMSE networks. In Section III-D, the proposed architecture is analyzed.

#### A. WMMSE Network

Let  $\mathcal{P} = (\{M_k, P_k, \mathcal{I}_k\}_{k=1}^K, \{N_i, \sigma_i^2, \alpha_i\}_{i=1}^I, \mathbb{H})$  be a tuple of wireless scenario parameters defining a network topology and channel conditions where  $\mathbb{H}$  describes a distribution of conforming channel matrix sets  $\{\mathbf{H}_{ik}\}_{i,k}$ . Let  $\mathcal{S} = (\mathcal{P}, \{\mathbf{H}_{ik}\}_{i,k})$  be a wireless scenario *realization* containing sampled channel matrices based on some scenario configuration  $\mathcal{P}$ , and let the beamformer achieving the maximum

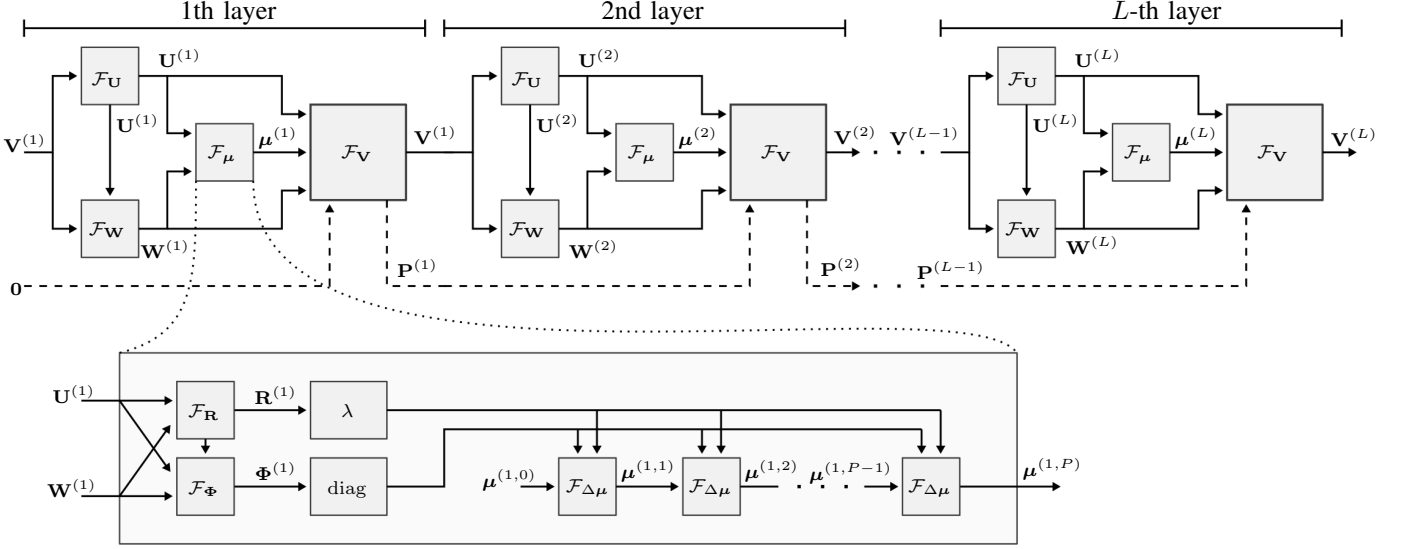


Figure 1. Deep network of the WMMSE algorithm obtained by unrolling  $L$  iterations. The blocks  $\mathcal{F}_U$ ,  $\mathcal{F}_W$  and  $\mathcal{F}_V$  represent the updates (3a), (3b) and (3d) for every  $i$ . The  $\mathcal{F}_\mu$ -block contains  $P$  root-finding iterations  $\mathcal{F}_{\Delta\mu}$  representing (9) for every  $k$ . The blocks  $\lambda$  and  $\text{diag}$  are the extraction of eigenvalues and diagonals respectively. The GCN-WMMSE architecture modifies the  $\mathcal{F}_W$ - and  $\mathcal{F}_V$ -blocks of the original algorithm. Dashed arrows represent the skip connections proposed in Section III-B4.

WSR be  $\mathcal{S}\mathbf{V}^{(\text{opt})} = \arg\max_{\mathbf{V}} \mathcal{R}_{\Sigma}(\mathbf{V}; \mathcal{S})$ . We seek a data-driven neural network model  $\mathcal{M}(\mathcal{S}; \mathbf{\Gamma})$  parameterized by a set of network parameters  $\mathbf{\Gamma}$  that approximates  $\mathcal{S}\mathbf{V}^{(\text{opt})}$  such that the expected rate over the distribution of scenarios is similar:

$$\mathbb{E}_{\mathcal{S} \sim p(\mathcal{S})} [\mathcal{R}_{\Sigma}(\mathcal{S}\mathbf{V}^{(\text{opt})}; \mathcal{S})] \approx \mathbb{E}_{\mathcal{S} \sim p(\mathcal{S})} [\mathcal{R}_{\Sigma}(\mathcal{M}(\mathcal{S}; \mathbf{\Gamma}); \mathcal{S})]. \quad (8)$$

The concept of unfolding entails adopting the architecture of a neural network from a hand-crafted iterative algorithm, then modifying and parameterizing it. By learning the optimal value of the network parameters from data, a network that is at least as performant as the original method while being computationally more efficient can be obtained [19], [20].

We base the architecture of GCN-WMMSE on  $L$  iterations of the WMMSE algorithm by interpreting each iteration with input  $\mathbf{V}^{(\ell-1)}$  and output  $\mathbf{V}^{(\ell)}$  as a neural network layer  $\mathcal{M}_u^{(\ell)}(\mathbf{V}; \mathcal{S})$ , such that the full network is the composition  $\mathcal{M}_u(\mathbf{V}; \mathcal{S}) = (\mathcal{M}_u^{(L)} \circ \mathcal{M}_u^{(L-1)} \circ \dots \circ \mathcal{M}_u^{(1)})(\mathbf{V}; \mathcal{S})$  w.r.t.  $\mathbf{V}$ . Figure 1 visualizes the forward pass of the resulting network. Each layer  $\mathcal{M}_u^{(\ell)}$  consists of the update blocks  $\mathcal{F}_W(\mathbf{V}; \mathcal{S})$ ,  $\mathcal{F}_U(\mathbf{V}, \mathbf{W}; \mathcal{S})$  and  $\mathcal{F}_V(\mathbf{U}, \mathbf{W}, \boldsymbol{\mu}; \mathcal{S})$ , which are the update mappings (3a), (3b) and (3d) for every UE  $i$ , and  $\mathcal{F}_\mu(\mathbf{U}, \mathbf{W}; \mathcal{S})$  which is (3c) for every BS  $k$ .

Previous works [23]–[25], [29] are restricted to less general wireless scenarios in order to unroll a simplified WMMSE network. For example, the utilization of KKT conditions is avoided by restricting to single-cell networks [24], or the optimization variables is made real and scalar by restricting to pairwise SISO links [25]. In our proposed network architecture in comparison, the general WMMSE algorithm is considered. Unfortunately, in this case the mapping  $\mathcal{F}_\mu$ , i.e., the solution to the problem in (3c), does not possess a closed-form solution in general. The iterative bisection search proposed in [5] to compute the optimum  $\mu_k^{(\ell, \text{opt})}$  is inadvisable since its accuracy is insufficient for a low number of subiterations  $P$  in the forward pass of the network. Instead, we propose to utilize

a method based on rational function approximations [30] to accelerate the forward pass of the WMMSE network and algorithm. At each substep  $p$  of the root-finding algorithm, an approximation  $\tilde{v}(\mu_k^{(\ell, p)}, \delta_N, \delta_D) = \delta_N / (\delta_D + \mu_k^{(\ell, p)})^2$  of (7) at the current iterate  $\mu_k^{(\ell, p)}$  is computed, where  $\tau$  and  $\delta$  are determined such that  $\tilde{v}(\mu_k^{(\ell, p)}, \delta_N, \delta_D) = v_k^{(\ell)}(\mu_k^{(\ell, p)})$  and  $\tilde{v}'(\mu_k^{(\ell, p)}, \delta_N, \delta_D) = v_k'^{(\ell)}(\mu_k^{(\ell, p)})$ . The non-negative intersection of  $\tilde{v}$  with 1 can be obtained in closed-form, leading to the update

$$\mu_k^{(\ell, p+1)} = \mu_k^{(\ell, p)} + 2 \frac{v_k^{(\ell)}(\mu_k^{(\ell, p)})}{v_k'^{(\ell)}(\mu_k^{(\ell, p)})} \left( 1 - \sqrt{v_k^{(\ell)}(\mu_k^{(\ell, p)})} \right) \quad (9)$$

which can be shown to converge monotonically to the root  $\mu_k^{(\ell, \text{opt})}$  if  $0 \leq \mu_k^{(\ell, p)} \leq \mu_k^{(\ell, \text{opt})}$ . If  $\mu_k^{(\ell, \text{opt})} < \mu_k^{(\ell, p)}$ , the iterate jumps to the interval  $(-\infty, \mu_k^{(\ell, \text{opt})})$  within a single iteration. Our simulations show that floating point precision is achieved after a low number of substeps  $P$ . To extend the solution to solve the problem in (3c),  $\mu_k^{(\ell, p)}$  is further mapped to 0 after each iteration if it is negative. The substeps (9) for every  $k$  are depicted as  $\mathcal{F}_{\Delta\mu}$ -blocks in Fig. 1.

## B. GCN-WMMSE Architecture

Depending on the scenario realization  $\mathcal{S}$ , the WMMSE network requires many layers to approach a local optimum. In this work we modify the  $\mathcal{F}_W$ -blocks and  $\mathcal{F}_V$ -blocks using concepts from graph convolutional filters (GCFs) and GCNs to significantly reduce the number of required layers while achieving beamformers of comparable quality. To this end, we first briefly introduce GCFs and GCNs in the following.

1) *Graph Convolutional Filters/Networks*: A GCF of order  $G$  is given as

$$\mathbf{f}_{\text{GCF}}(\mathbf{x}; \mathbf{S}, \{a_g\}_{g=0}^G) = \sum_{g=0}^G a_g \mathbf{S}^g \mathbf{x}, \quad (10)$$

where  $a_g$  for  $g = 0, \dots, G$  are filter taps. The matrix  $\mathbf{S} \in \mathbb{R}^{M \times M}$  is a shift matrix which describes the progression of a graph signal  $\mathbf{x} \in \mathbb{R}^M$  between two discrete time steps.

GNNs are an extension to graph filters which enable a multilayer design by introducing nonlinearities with multiple parallel filters similar to convolutional neural networks. A single layer of a GCN, a common variant of a GNN, can be expressed as

$$\mathbf{F}_{\text{GCN}}(\mathbf{X}; \mathbf{S}, \{\mathbf{A}_g\}_{g=0}^G, \mathbf{b}) = \phi \left( \sum_{g=0}^G \mathbf{S}^g \mathbf{X} \mathbf{A}_g + \mathbf{1} \mathbf{b}^T \right). \quad (11)$$

Equation (11) maps a signal  $\mathbf{X} \in \mathbb{R}^{N \times F_1}$  containing  $F_1$  features to an output of size  $N \times F_2$  with  $F_2$  features. The matrices  $\mathbf{A}_g \in \mathbb{R}^{F_1 \times F_2}$  for  $g = 0, \dots, G$  store the filter coefficients. In conjunction with a biasing parameter  $\mathbf{b} \in \mathbb{R}^F$ , an elementwise nonlinearity  $\phi$  furthers expressiveness of the mapping, allowing for higher selectivity by frequency mixing while maintaining stability to errors [31]. Please refer to [32], [33] for more details. In the following, we unfold the  $\mathcal{F}_{\mathbf{W}}$ - and  $\mathcal{F}_{\mathbf{V}}$ -blocks.

2) *Weight Matrix Graph Filter*: The idea of graph filtering is extended to the complex domain and applied to the  $\mathcal{F}_{\mathbf{W}}$ -block. To this end, we consider the original weight matrix update in (3b)  $\hat{\mathbf{W}}^{(\ell)} = \left( \mathbf{I} - (\mathbf{V}_i^{(\ell-1)})^H \mathbf{H}_{ik}^H \mathbf{U}^{(\ell)} \right)^{-1}$ , where  $i \in \mathcal{I}_k$ , as a shift matrix and introduce the weight matrix GCF

$$\mathbf{W}_i^{(\ell)} = a_{W,\ell 0} \mathbf{I} + \sum_{g=1}^G \frac{a_{W,\ell g}}{\left( \text{Tr} \left\{ \hat{\mathbf{W}}_i^{(\ell)} \right\} / N_i \right)^{g-1}} \left( \hat{\mathbf{W}}_i^{(\ell)} \right)^g \quad (12)$$

of order  $G$  for every  $i$ , where  $a_{W,\ell g}$  for  $g = 0, \dots, G$  and  $\ell = 1, \dots, L$ , are learnable filter taps. Thus, (12) replaces the standard WMMSE weight update. The filter taps  $a_{W,\ell g}$  are restricted to be non-negative ( $a_{W,\ell g} \geq 0$ ) to ensure that  $\mathbf{W}_i^{(\ell)}$  is PSD. The mean of eigenvalues  $\text{Tr} \left\{ \hat{\mathbf{W}}_i^{(\ell)} \right\} / N_i$  normalizes the filter taps for  $g \geq 2$  to prevent numerical issues in case of a high signal-to-noise ratio (SNR). It can be shown that an equal scaling transformation of  $\mathbf{W}_i^{(\ell)}$  for all  $i$  does not change the output of a layer  $\ell$  if the following update blocks follow the normal WMMSE updates. However, this scaling ambiguity can be prevented by fixing one filter tap  $a_{W,\ell g}$ , or a modification of the subsequent  $\mathcal{F}_{\mathbf{V}}$ -block as outlined below.

3) *Downlink Graph Convolutional Neural Network*: The  $\mathbf{V}$ -step in (3d) can be interpreted as a GCF with the pseudoinverse of the modified weighted uplink covariance matrix  $\tilde{\mathbf{R}}_k^{(\ell)} = \mathbf{R}_k^{(\ell)} + \mu_k^{(\ell,P)} \mathbf{I}$  in (4) as shift operator. The filter acting on the candidate beamformer  $\tilde{\mathbf{V}}_i^{(\ell)}$  in (5) is then extended into a complex-valued GCN layer with  $F$  features as in (11), leading to the modified  $\mathbf{V}$ -update obtaining the unscaled beamformer  $\hat{\mathbf{V}}_i$

$$\hat{\mathbf{v}}_{id}^{(\ell)} = \text{modReLU} \left( \tilde{\mathbf{P}}_{id}^{(\ell)}, \frac{1}{b_S} \sqrt{\frac{P_k}{|\mathcal{I}_k|}} \mathbf{1} \mathbf{b}_\ell^T \right) \mathbf{c}_\ell$$

where  $\tilde{\mathbf{P}}_{id}^{(\ell)} = (\tilde{\mathbf{R}}_k^{(\ell)})^\dagger \tilde{\mathbf{v}}_{id}^{(\ell)} \mathbf{a}_{V,\ell 1}^T + \tilde{\mathbf{v}}_{id}^{(\ell)} \mathbf{a}_{V,\ell 0}^T \quad (13)$

for every  $i \in \mathcal{I}_k$  for all  $k$ , where  $\tilde{\mathbf{v}}_{id}^{(\ell)}$  and  $\hat{\mathbf{v}}_{id}^{(\ell)}$  for  $d = 1, \dots, N_i$  are the columns/streams in  $\tilde{\mathbf{V}}_i^{(\ell)} = [\tilde{\mathbf{v}}_{i1}^{(\ell)}, \dots, \tilde{\mathbf{v}}_{iN_i}^{(\ell)}]$

and  $\hat{\mathbf{V}}_i^{(\ell)} = [\hat{\mathbf{v}}_{i1}^{(\ell)}, \dots, \hat{\mathbf{v}}_{iN_i}^{(\ell)}]$ . The GCN layer corresponds to a filter of polynomial degree 1 with  $\mathbf{a}_{V,\ell 1} \in \mathbb{C}^F$  and  $\mathbf{a}_{V,\ell 0} \in \mathbb{C}^F$  being trainable complex filter taps,  $\mathbf{b}_\ell \in \mathbb{R}^F$  being an additional trainable bias, and  $\mathbf{c}_\ell \in \mathbb{C}^F$  is a trainable vector recombining the  $F$  features contained in  $\tilde{\mathbf{P}}_{id}^{(\ell)}$ . Higher polynomial orders empirically do not provide any benefits. The bias is scaled by the power and number of assigned UEs in order to improve the generalization performance. The auxiliary scaling parameter  $b_S$  reduces the magnitude of the bias term relative to the other summands, while maintaining the flexibility for different numbers of assigned UEs and power changes. This becomes necessary when applying an optimizer like ADAMW [34] to prevent bias parameters steps having a too dominant impact compared to other parameters. modReLU is a complex variant of the rectified linear unit (ReLU) [35] and is defined as

$$\text{modReLU}(x, b) = \begin{cases} (|x| + b) \frac{x}{|x|}, & \text{for } |x| + b > 0 \\ 0, & \text{otherwise.} \end{cases} \quad (14)$$

The nonlinearity (14) empirically performs better than applying a ReLU to the real and imaginary components individually. The architecture is limited to single-layer GCNs since the benefit of multiple layers has been contested [36]. Furthermore, applying multi-layer GCNs does not yield an empirical improvement for GCN-WMMSE. Since adherence to the power constraints cannot be guaranteed by the GCN, an additional power projection step

$$\mathbf{V}_i^{(\ell)} = \sqrt{P_k} \hat{\mathbf{V}}_i^{(\ell)} / \sqrt{\max \left\{ \sum_{i \in \mathcal{I}_k} \left\| \hat{\mathbf{V}}_i^{(\ell)} \right\|_F^2, P_k \right\}}, \quad (15)$$

for all  $i$  is introduced as a post-processing step of the output of each  $\mathcal{F}_{\mathbf{V}}$ -block. Sets of beamforming matrices  $\{\hat{\mathbf{V}}_i^{(\ell)}\}_{i \in \mathcal{I}_k}$  exceeding the maximum power  $P_k$  are projected onto the feasible set, while feasible beamformer sets are preserved.

4) *Skip Connections*: Lastly, we adopt the concept of additional connections between layers that has been successfully applied in residual and highway networks [37]–[39]. Specifically, the input to the modReLU nonlinearity  $\tilde{\mathbf{P}}_{id}^{(\ell)}$  is replaced by  $\mathbf{P}_{id}^{(\ell)} = \tilde{\mathbf{P}}_{id}^{(\ell)} + \mathbf{P}_{id}^{(\ell-1)} \mathbf{D}_\ell$ . A trainable mapping matrix  $\mathbf{D}_\ell \in \mathbb{C}^{F \times F}$  allows for linear combinations of the features of the previous layer. Thus, a direct path for the additional exchange of gradient information between layers is created, bypassing operations such as matrix inversions which sometimes lead to noisy gradients. The additional network connections are illustrated in Fig. 1 as dashed arrows.

5) *Initialization Beamformers*: The function generating the initial beamformer set  $\mathbf{V}^{(0)}$  that is fed into the input of the network needs to be integrated into the network models themselves since the optimal values of the trainable parameters depend on it. In this work we only consider initialization functions which are entirely determined by the scenario realization  $\mathcal{S}$  without any additional trainable parameters. We thus obtain deep networks  $\mathcal{M}(\mathcal{S}; \Gamma)$  with a trainable parameter set  $\Gamma$  containing in total  $\{\mathbf{a}_{V,\ell 1}\}_{\ell=1}^L, \{\mathbf{a}_{V,\ell 0}\}_{\ell=1}^L, \{\mathbf{b}_\ell\}_{\ell=1}^L, \{\mathbf{c}_\ell\}_{\ell=1}^L, \{\mathbf{D}_\ell\}_{\ell=2}^L$  and  $\{\{a_{W,\ell g}\}_{g=0}^G\}_{\ell=1}^L$  in case of  $L$  layers ( $b_S$  is separately treated as discussed in Section III-C).

### C. Model Training

Optimizing the trainable parameter set  $\mathbf{\Gamma}$  of a GCN-WMMSE network with  $L$  layers is achieved by the maximization of the expected rate in (8). In practice, the expectation needs to be approximated by a finite data set  $\mathcal{T}$  and the non-convex optimization is classically performed by SGD. In this work, we perform SGD for  $T$  steps by descending along the gradient  $\nabla_{\mathbf{\Gamma}} J(\mathcal{T}_t; \mathbf{\Gamma}, \mathcal{L})$  of the sample-normalized loss function

$$J(\mathcal{T}_t; \mathbf{\Gamma}, \mathcal{L}) = \frac{1}{|\mathcal{T}_t| |\mathcal{L}|} \sum_{\mathcal{S}_n \in \mathcal{T}_t} \sum_{\ell \in \mathcal{L}} \frac{J_{\text{WSR}}^{(\ell)}(\mathcal{S}_n; \mathbf{\Gamma})}{r_{n,\mathbf{\Gamma}}^{(\ell)}}, \quad (16)$$

where  $\mathcal{L}$  is a set of layers and  $\mathcal{T}_t$  is a minibatch of scenario realizations  $\mathcal{S}_n$  at training step  $t$ . The partial loss  $J_{\text{WSR}}^{(\ell)}$  is the negative WSR achieved on the realization  $\mathcal{S}_n$  with the downlink beamformer set  $\mathbf{V}^{(\ell)}$  computed by the  $\ell$ -th network layer given a set of network parameters  $\mathbf{\Gamma}$ , i.e.,  $J_{\text{WSR}}^{(\ell)}(\mathcal{S}_n; \mathbf{\Gamma}) = -\mathcal{R}_{\Sigma}(\mathcal{M}^{(1:\ell)}(\mathcal{S}_n; \mathbf{\Gamma}); \mathcal{S}_n)$  where  $\mathcal{M}^{(1:\ell)}$  denotes the neural network up to layer  $\ell$ . The scalar  $r_{n,\mathbf{\Gamma}}^{(\ell)}$  is determined as the magnitude of  $J_{\text{WSR}}^{(\ell)}(\mathcal{S}_n; \mathbf{\Gamma})$  in the forward pass. It equalizes the loss per sample to unity but is otherwise treated as scaling in the gradient computation. Thus, realizations with lower achievable WSR have the same impact on the gradient as realizations with high WSR. Equation (16) generalizes the loss function utilized in [14] for multiple output layers. The scaling parameter  $b_S$  in (13) is obtained during training by a running mean of the empirical expectation  $\mathbb{E}_{\mathcal{S} \sim \mathcal{T}} \left[ \sqrt{\frac{P_k}{|\mathcal{Z}_k|}} \right]$  dependent on the power budget of scenarios in the training set  $\mathcal{T}$ .

SGD involves the full complex gradient w.r.t. the parameters in  $\mathbf{\Gamma}$  which is typically obtained by backpropagation. Since this requires the full Jacobian w.r.t. the inputs of the update blocks, e.g.,  $\mathbf{V}$  and  $\mathbf{W}$  in case of the  $\mathcal{F}_{\mathbf{W}}$ -block, the existence of the partial derivatives must be ensured. This is straightforward for all matrix operations in the GCN-WMMSE architecture, and workarounds for pointwise non-differentiable nonlinearities are well investigated. However, naive backpropagation of multiple concatenated update steps (9) in the  $\mathcal{F}_{\mu}^{(\ell)}$ -block to obtain the derivative w.r.t. the eigenvalues of  $\mathbf{R}_k^{(\ell)}$  and the diagonal values  $\varphi_{km}^{(\ell)}$ , while feasible in practice, is prone to numerical issues as it involves divisions by small numbers. Instead, an efficient and exact gradient of the entire update block  $\mathcal{F}_{\mu}$  assuming a fully converged iterate can be obtained within a single step.

**Proposition 1.** Let  $\mu_k^{(\ell, \text{opt})} = f(\mathbf{z}_k^{(\ell)})$  where  $\mathbf{z}_k^{(\ell)} = \left( \left\{ \varphi_{km}^{(\ell)} \right\}_{m=1}^M, \left\{ \lambda_{km}^{(\ell)} \right\}_{m=1}^M \right)$  be the function that is implicitly defined as the solution of (3c). For any point  $\tilde{\mathbf{z}}_k^{(\ell)}$  with  $\tilde{\varphi}_{km}^{(\ell)} > 0$  and  $\tilde{\lambda}_{km}^{(\ell)} > -\tilde{\mu}_k^{(\ell, \text{opt})}$ : The gradient of  $f$  at  $\tilde{\mathbf{z}}_k^{(\ell)}$  exists if  $\tilde{\mu}_k^{(\ell, \text{opt})} > 0$  and

$$\begin{aligned} \frac{\partial}{\partial \varphi_{ki}^{(\ell)}} f(\tilde{\mathbf{z}}_k^{(\ell)}) &= \frac{(\tilde{\lambda}_{ki}^{(\ell)} + \tilde{\mu}_k^{(\ell, \text{opt})})^{-2}}{2 \sum_{m=1}^{M_k} \frac{\tilde{\varphi}_{km}^{(\ell)}}{(\tilde{\lambda}_{km} + \tilde{\mu}_k^{(\ell, \text{opt})})^2}}, \\ \frac{\partial}{\partial \lambda_{ki}^{(\ell)}} f(\tilde{\mathbf{z}}_k^{(\ell)}) &= -\frac{\tilde{\varphi}_{ki}^{(\ell)} (\tilde{\lambda}_{ki}^{(\ell)} + \tilde{\mu}_k^{(\ell, \text{opt})})^{-3}}{\sum_{m=1}^{M_k} \frac{\tilde{\varphi}_{km}^{(\ell)}}{(\tilde{\lambda}_{km} + \tilde{\mu}_k^{(\ell, \text{opt})})^2}}. \end{aligned} \quad (17)$$

Furthermore, for  $\tilde{\mu}_k^{(\ell, \text{opt})} = 0$  with  $\sum_{m=1}^M \frac{\tilde{\varphi}_{km}^{(\ell)}}{(\tilde{\lambda}_{km} + \tilde{\mu}_k^{(\ell, \text{opt})})^2} \neq 1$ , the gradient exists and is given by

$$\frac{\partial}{\partial \varphi_{ki}^{(\ell)}} f(\tilde{\mathbf{z}}_k^{(\ell)}) = 0 \quad \text{and} \quad \frac{\partial}{\partial \lambda_{ki}^{(\ell)}} f(\tilde{\mathbf{z}}_k^{(\ell)}) = 0. \quad (18)$$

A proof is obtained by applying [40, Thm. 8.2] to the complementary slackness condition (6). Since the derivative is undefined in the point where  $\mu^{(\ell, \text{opt})} = 0$  with  $\sum_{m=1}^{M_k} \frac{\tilde{\varphi}_{km}^{(\ell)}}{(\tilde{\lambda}_{km} + \tilde{\mu}_k^{(\ell, \text{opt})})^2} = 1$ , it has to be extended in practice. In our implementation, it is set to 0 in this case. Furthermore, the exact solution  $\tilde{\mu}_k^{(\ell, \text{opt})}$  has to be replaced by the iterate  $\tilde{\mu}_k^{(\ell, P)}$ . Note that a closed-form expression only exists for the derivative of the implicit function  $f$ . In the forward pass of the network, a closed-form expression of  $f$  does not exist and the iterative procedure with updates in (9) is used instead.

### D. Discussion

Unfolding leads to a highly structured neural network with usually a low number of trainable parameters. In the case of the GCN-WMMSE architecture, the network models only contain  $L(4F + G + 1) + (L - 1)F^2$  trainable parameters, which reduces the risk of overfitting and dramatically increases the data efficiency, as will be demonstrated in Section IV. Furthermore, it can be shown that the original WMMSE is contained in the family of functions spanned by the GCN-WMMSE architecture.

Since GCN-WMMSE does not introduce additional quantities that need to be shared between consecutive update operations, with the exception of  $\mathbf{P}_{id}^{(\ell)}$  which remains local at a BS, no additional information needs to be exchanged between UEs and BSs at test time compared to the WMMSE. Thus, assuming that the model parameters in  $\mathbf{\Gamma}$  are already known throughout the network, GCN-WMMSE inherits the capability of distributed deployment from the WMMSE algorithm. In this scenario, BSs only need to share  $G + 1$  parameters with the UEs beforehand.

The application of GCFs and GCNs to unfold the WMMSE algorithm inherits multiple favorable properties of those structures. Firstly, GCFs and GCNs exhibit permutation equivariance: Consider an arbitrary permutation matrix  $\mathbf{\Pi} \in \{0, 1\}^{N \times N}$  fulfilling  $\mathbf{\Pi} \mathbf{1} = \mathbf{\Pi}^T \mathbf{1} = \mathbf{1}$  and a GCF as in (10), then  $\mathbf{f}_{\text{GCF}}(\mathbf{x}; \mathbf{S}, \{a_g\}_{g=0}^G) = \mathbf{\Pi} \mathbf{f}_{\text{GCF}}(\mathbf{\Pi}^T \mathbf{x}; \mathbf{\Pi}^T \mathbf{S} \mathbf{\Pi}, \{a_g\}_{g=0}^G)$ . The same holds for GCN layers such as (11). Consequently, relabeling of the nodes of a graph, which is equivalent to a permutation of the signal vector and equal permutation of the rows and columns of the shift matrix, does not change the output apart from said permutation. Permutation equivariance w.r.t. relabeling of the transceiver antennas is a natural property of a wireless network if no additional assumptions are made, and it is replicated by the original matrix filter operations of the WMMSE algorithm. Replacing those with GCFs or GCNs preserves this natural property in the GCN-WMMSE architecture; the proof is straightforward but is omitted for lack of space. Permutation equivariance w.r.t. relabeling of the network participants as emphasized in [25] is automatically achieved if all BSs and UEs share the same neural network parameters.

Secondly, the filter matrix resulting from the GCFs polynomial on the shift matrix  $\mathbf{S}$  as in (10) has the same eigenbasis as  $\mathbf{S}$ , but its eigenvalues are mapped by the polynomial with coefficients  $\{a_g\}_{g=0}^G$ . In case of the weight matrix update  $\mathcal{F}_{\mathbf{W}}$  (12), the coefficients of the polynomial in  $\hat{\mathbf{W}}_i^{(\ell)}$ , which is the inverse of the receiver symbol error matrix  $\mathbf{E}_i^{(l)}$ , are non-negative. Considering a degree  $G \geq 2$ , this leads to an amplification of large eigenvalues corresponding to low error eigenspaces and an attenuation of small eigenvalues corresponding to high error eigenspaces compared to a polynomial of degree  $G = 1$ . Thus, when forming the candidate beamformer matrix  $\tilde{\mathbf{V}}_i$  in (5) using  $\mathbf{W}_i^{(\ell)}$ , the GCF acts as a highpass on the eigenvalues and corresponding signal spaces of the virtual uplink precoder  $\alpha_i(\mathbf{U}_i^{(\ell)})^H \mathbf{H}_{ik}$  which belong to low error receive symbol spaces in  $\mathbf{E}_i^{(l)}$ . Similarly, the significant interference eigenspaces of the weighted uplink covariance  $\mathbf{R}_k^{(\ell)}$  (4) are amplified due to the weight matrix GCF as well. In the downlink beamformer update  $\mathcal{F}_{\mathbf{V}}$ , the signal components of the candidate beamformer  $\tilde{\mathbf{V}}_i$  are then filtered according to the eigenvalues of  $\tilde{\mathbf{R}}_k^{(\ell)}$ . The property is known as interference avoidance and it is performed by the WMMSE algorithm as well as the proposed architecture both at the transmitter on the basis of the reciprocal channel and at the receiver. This scheme originates from cooperative approaches with the goal of interference alignment [41], [42], which is optimal for high SNR. The WMMSE algorithm is similarly structured compared to algorithms which relax this goal [43]. The downlink beamformer update  $\mathcal{F}_{\mathbf{V}}$  in (13) is a trainable interference avoidance filter which directly leverages this notion. The GCN provides additional degrees of freedom compared to a GCF and simultaneously offers a higher selectivity due to the nonlinearity as well as resilience to errors [31]. Both (12) and (13) are optimized w.r.t. the global objective compared to the locally optimal operations (3b) and (3d) invoked by BCD, thus achieving interference avoidance that is superior for the global WSR objective.

Lastly, the applied GCFs and GCNs enable a high transferability regarding wireless scenario configurations. GCN-WMMSE networks are transferable to *any* set of scenario configurations for any given set of trainable parameters. Therefore, it is more general than all previous works on unfolding the WMMSE. This, together with the parameter efficiency, can be leveraged in distributed training schemes such as federated learning. The generality of the model addresses the fundamental problem of heterogeneous data in federated learning and the low number of parameters increases the efficiency when exchanging model parameters or gradients.

The proposed GCN-WMMSE architecture adds  $\mathcal{O}(I(G-1)N^3 + IF^2NM + INM)$  of per-iteration complexity over the classical WMMSE algorithm, where  $N$  and  $M$  are the number of antennas of each UE or BS, respectively. However, the increase is absorbed into the WMMSE per-iteration complexity  $\mathcal{O}(I^2N^2M + KIN^2M + INM^2 + IN^3 + KM^3)$ , since  $F$  and  $G$  are constant w.r.t. the scenario. Thus, the impact of the additional operations is low, which is verified by experiments.

Table I  
BASE PARAMETER SET FOR GCN-WMMSE NETWORKS AND GENERAL TRAINING PARAMETERS.

Base Model Hyperparameters	
Number of Layers $L$	7
Polynomial Degree $G$	2
Number of Filters $F$	4
Base Training Hyperparameters	
Loss Function	(16) with $\mathcal{L} = \{L\}$
ADAMW $(\beta_1, \beta_2, \lambda)$	(0.9, 0.99, $10^{-3}$ )
Learning Steps $T$	$10^4$
Learning Rate $\eta$	0.01, /10 after every 2500 steps
Minibatch Size $ \mathcal{T}_t $	100
Gradient Clipping Value	1

Table II  
BASE SCENARIO CONFIGURATION FOR THE VALIDATION AND TRAINING SCENARIO SAMPLES.

Base Scenario Configuration	
BS Distance $d_{\text{BS}}$	200 m
BS Antenna Dimension $M$	12
BS Tx Power $P_{\text{BS}}$	30 dBm
Num. of UEs $I$	12, equal num. assigned per BS
UE Antenna Dimension $N$	2
UE Noise Power $\sigma_{\text{UE}}^2$	-100 dBm

#### IV. EXPERIMENTS AND DISCUSSION

In this section, we evaluate the performance of the proposed GCN-WMMSE architecture with special focus on carving out its generalization capabilities, then we verify the application of those characteristics. All models and algorithms are implemented<sup>2</sup> using PyTorch [44]. We apply SGD and leverage the AdamW optimizer [34]. In Section IV-A and IV-B, GCN-WMMSE network models are assessed on an artificial scenario of 3 BSs positioned at the corners of an equilateral triangle of side length  $d_{\text{BS}}$ , similar to [45] without directional antennas. For each channel realization, all UEs are randomly and uniformly placed inside the sextant centered on their assigned BS with radius  $d_{\text{BS}}/\sqrt{3}$ . The large-scale path loss  $PL_{ik}$  between BS  $k$  and UE  $i$  is calculated according to the picocell model [46]. We assume a rich scattering environment for both the BSs and UEs and Rayleigh fading. Thus, the channel matrix coefficients  $[\mathbf{H}_{ik}]_{nm}$  are sampled from  $\mathcal{CN}(0, 10^{\frac{PL_{ik}}{10}})$ . In Section IV-C and Section IV-D, the DeepMIMO dataset [47] is leveraged instead. For simplicity, we assume equal UE antennas dimensions  $N_i = N$ , UE noise variances  $\sigma_i^2 = \sigma_{\text{UE}}^2$ , sum-rate weights  $\alpha_i = 1$ , BS antenna dimensions BS  $M_k = M$  and BS power budget  $P_k = P_{\text{BS}}$ . Similarly, an equal amount of UEs  $|\mathcal{I}_k| = \mathcal{I}$  is assigned to each individual BS, however, GCN-WMMSE exhibits comparable performance if  $|\mathcal{I}_k|$  is not equal for all  $k$ .

All experiments from Section IV-A to IV-D are conducted using the network and training hyperparameters summarized in Tab. I, unless specified otherwise. The filter taps of the downlink beamformer GCNs are initialized according to [35], the biases with  $\mathbf{0}$  and the taps of the weight GCFs by  $1/(G+1)$ . GCN-WMMSE is initialized by normalized maximum-ratio

<sup>2</sup>To promote reproducible research, the code is publicly available at <https://github.com/lsky96/gcnwmmse>.

Table III  
OVERVIEW OF COMPARED ALGORITHM AND MODEL VARIANTS.

Acronym	Explanation
<b>GCN-WMMSE</b>	Proposed architecture...
MT	...trained on scenarios configured as in test set.
PT	...trained on scenario configuration marked by arrow.
DT	...trained on random scenario configuration.
<b>WMMSE</b>	Baseline algorithm...
RI	...with random initializations.
RI TR	...with random initializations truncated to $L$ iterations.
50	...with best result of 50 initializations
MRC	...with MRC initialization.
MRC TR	...with MRC initialization truncated to $L$ iterations.

Table IV  
ABSOLUTE AND RELATIVE RATE OF THE PROPOSED GCN-WMMSE NETWORKS COMPARED TO WMMSE50 OVER NETWORK DEPTHS  $L$ .

Number of Layers $L$	3	4	5	6	7	8	9
Abs. Rate $\mathcal{R}_\Sigma (\frac{\text{nat}}{\text{Hz}})$	82.21	87.84	89.98	91.67	92.56	93.46	93.89
Rel. Rate $\mathcal{R}_\Sigma^{\text{rel.}} (\%)$	83.72	89.45	91.63	93.35	94.26	95.17	95.61

combining (MRC) beamformers  $\mathbf{V}_i^{(0)} \propto \mathbf{H}_{ik}^H$  for  $i \in \mathcal{I}_k$ . The Lagrangian variable is initialized as  $\mu_k^{(\ell,0)} = 10^{-12}$  for every  $\ell$  and updated for  $P = 8$  iterations. The validation sets contain 1000 scenario realizations but the training samples are 'single-use' and newly sampled at each step  $t$ , unless specified otherwise. We compare to the classical WMMSE algorithm. WMMSE RI denotes the WSR achieved by the WMMSE algorithm averaged over 50 random initializations per scenario realization. Random beamformer initializations are obtained by sampling the matrix elements from  $\mathcal{CN}(0, 1)$  and normalization such that the power constraints are exactly met. We earmark WMMSE50 as the best WSR achieved by the WMMSE algorithm over these 50 initializations. It serves as a benchmark, however, we remark that it is impractical due to its high computational cost. WMMSE MRC denotes the WMMSE algorithm initialized by MRC beamformers. The WMMSE algorithm is always carried out for 100 iterations. The acronym TR indicates the average rate that the WMMSE algorithm achieves when being truncated after  $L$  iterations, therefore, requiring the same communication overhead as GCN-WMMSE. The average achievable WSR is denoted by  $\mathcal{R}_\Sigma$ , and  $\mathcal{R}_\Sigma^{\text{rel.}}$  denotes the average WSR relative to the result of WMMSE50 in percent. Tab. III provides an overview over the variants of the algorithm and the proposed model.

#### A. General Performance and Ablation Study

In this section, GCN-WMMSE networks are trained and validated on scenarios configured as in Tab. II.

1) *Number of Network Layers  $L$* : Tab. IV shows that the rate of the proposed GCN-WMMSE increases consistently from 3 to 9 network layers up to 95.61% relative WSR, however, there are significant diminishing returns after about 6 layers. Nevertheless, since WMMSE RI achieves 95.20% relative WSR only after 100 iterations, the results prove that the computation time and iterations can be drastically reduced. We select  $L = 7$  for the following experiments.

2) *Number of GCN Filter Features  $F$* : Tab. V shows that increasing the number of GCN filters  $F$  in each layer only

Table V  
RATE AND RELATIVE RATE OF THE PROPOSED GCN-WMMSE NETWORKS COMPARED TO WMMSE50 FOR DIFFERENT NUMBERS OF FILTERS  $F$ .

Number of Filters $F$	1	2	4	6
Abs. Rate $\mathcal{R}_\Sigma (\frac{\text{nat}}{\text{Hz}})$	91.49	92.08	92.56	92.56
Rel. Rate $\mathcal{R}_\Sigma^{\text{rel.}} (\%)$	93.16	93.77	94.26	94.26

Table VI  
ABLATION STUDY OF THE ARCHITECTURE COMPONENTS OF GCN-WMMSE (PROPOSED).

Changed Component	$\mathcal{R}_\Sigma (\frac{\text{nat}}{\text{Hz}})$	$\mathcal{R}_\Sigma / \mathcal{R}_{\Sigma, \text{Base}} (\%)$
Base	92.56	100.00
w/o Weight Matrix GCF	91.72	99.09
w/o Skip Connections	87.53	94.57
w/o Biasing/modReLU	89.20	96.37
w/o Diagonal Loading	92.70	100.15
w/ MA	92.39	99.81

yields a marginal increase in the WSR. An increase of  $F$  is, however, associated with an increase in the number of 'good' filter initializations, which leads to accelerated and stabilized training as Fig. 2 demonstrates.

3) *Ablation Study*: In Tab. VI, individual network components are added or removed one at a time to study their impact on the WSR at the last layer. In case of the weight matrix GCF (c.f. (12)), it is replaced by the original WMMSE update (3b). *Diagonal Loading* and *Biasing* refers to the terms with the parameters  $\mathbf{a}_{V, \ell 0}$  and  $\mathbf{b}_\ell$  in (13). MA (moving average) refers to an additional term in (13) containing the non-inverted loaded weighted uplink covariance matrix  $\tilde{\mathbf{R}}_k^{(\ell)}$ , i.e., we have  $\tilde{\mathbf{P}}_{id}^{(\ell)} = (\tilde{\mathbf{R}}_k^{(\ell)})^\dagger \tilde{\mathbf{v}}_{id}^{(\ell)} \mathbf{a}_{V, \ell 1}^\top + \tilde{\mathbf{v}}_{id}^{(\ell)} \mathbf{a}_{V, \ell 0}^\top + \tilde{\mathbf{R}}_k^{(\ell)} \tilde{\mathbf{v}}_{id}^{(\ell)} \mathbf{a}_{\text{ma}, \ell}^\top$  with an additional trainable parameter  $\mathbf{a}_{\text{ma}, \ell} \in \mathbb{C}^F$ .

The results are given in Tab. VI and have a two-sided 99%-confidence of  $\pm 0.1 \frac{\text{nat}}{\text{Hz}}$ . The biasing, which activates the modReLU-nonlinearity, and the skip connections have the largest performance impact. The effectiveness of skip connections is due to a significant acceleration and stabilization in training [37], [38] as shown in Fig. 2. The weight matrix GCF has a statistically significant though comparably low impact. Its computational cost, however, is low and it can be empirically shown that it becomes more advantageous for higher SNR. On the other hand, the results suggest that the diagonal loading term could be detrimental. Adding an MA-term does not improve the performance in this setup.

4) *Loss Layer Set  $\mathcal{L}$* : Fig. 3 investigates the impact of the choice of layers  $\ell$  in the layer set  $\mathcal{L}$  considered in the loss function in (16). When performing greedy SGD on all layers, a rate of  $81.71 \frac{\text{nat}}{\text{Hz}}$  (83.21% compared to WMMSE50) is achieved after only 3 layers, WMMSE RI requires 8 iterations to achieve a similar result. However, the network performance saturates as the greedy method risks slipping into inferior local optima, while  $\mathcal{L} = \{L\}$  eventually achieves a higher rate of  $92.56 \frac{\text{nat}}{\text{Hz}}$  (compared to  $89.81 \frac{\text{nat}}{\text{Hz}}$ ). In a deployment scenario with a flexible runtime or number of feedback loops, i.e. exchanges between transmitters and receivers, the algorithm may be terminated early after a few layers. Therefore, the trade-off in choosing  $\mathcal{L}$  is important to consider.



Table VII  
ABSOLUTE AND RELATIVE WSR OF GCN-WMMSE (PROPOSED) FOR A FINITE SET OF TRAINING SAMPLES.

Training Set Size $ T $	100	200	300	400	500	600	700	800	900	1000
Abs. Rate $\mathcal{R}_\Sigma$ ( $\frac{\text{nat}}{\text{Hz}}$ )	91.58	91.82	91.73	92.06	92.17	92.08	92.09	92.28	92.50	92.16
Rel. Rate $\mathcal{R}_\Sigma^{\text{rel}}$ (%)	93.26	93.50	93.41	93.75	93.85	93.77	93.78	93.97	94.19	93.84

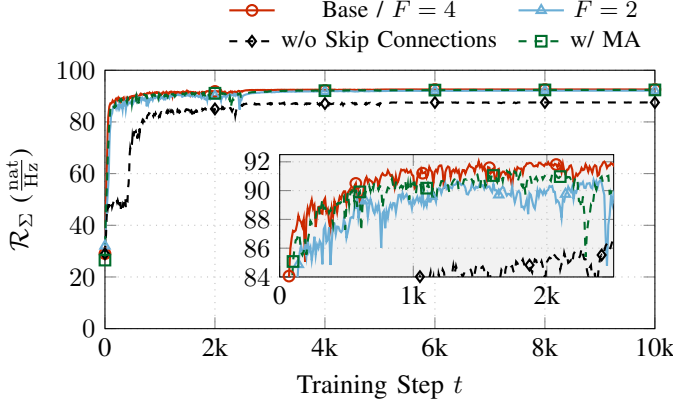


Figure 2. Convergence of GCN-WMMSE models evaluated on validation set over  $T$  training steps.

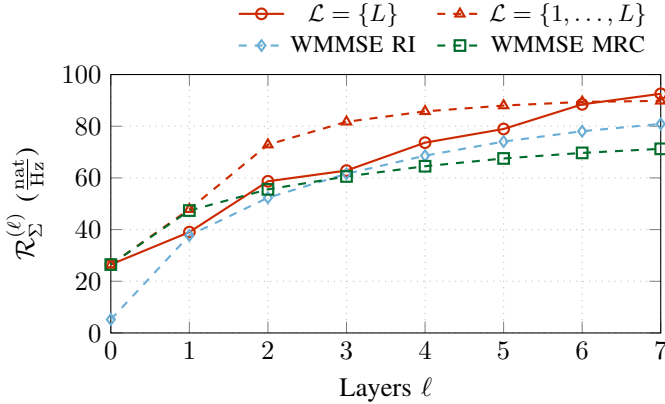


Figure 3. Performance of GCN-WMMSE (proposed) given the layer outputs  $\mathbf{V}_i^{(\ell)}$  for a network with  $L = 7$  layers. The loss (16) is based on the output of either the last or all layers.

5) *Training Data Set Size  $|T|$* : Finally, instead of training data being generated on demand, a finite training data set is considered in Tab. VII. We observe that for a data set size of 100 scenario samples the relative WSR already achieves a value of 93.26%. This remarkable data efficiency is enabled by the equivariance properties of the graph filter structures and the preservation of the original WMMSE algorithm structure. The number of parameters is low with only 229 scalar network parameters in this example.

Table VIII  
COMPARISON OF COMMUNICATION OVERHEAD AND COMPUTATIONAL COST BETWEEN GCN-WMMSE (PROPOSED) AND WMMSE ALGORITHM.

# Communication Rounds		Computational Cost [ms]	
GCN-WMMSE	WMMSE RI	GCN-WMMSE	WMMSE RI
6	42	3.07	17.82
7	63	3.57	26.70
8	98	4.12	41.83

6) *Computational Cost and Communication Overhead*: We compare the computational cost and communication overhead of GCN-WMMSE for  $L = 6, 7, 8$  against WMMSE RI with a number of iterations that achieves a comparable WSR on the base scenario. Note that the communication overhead is proportional to the number of required communication rounds, which itself is equal to the number of layers/iterations. The computational cost is given for a centralized execution with a AMD R7 2700X CPU with 32GB memory.

Tab. VIII demonstrates that GCN-WMMSE reduces the computational cost by a factor of 6 up to 10, with the relative advantage increasing for deeper networks. Simultaneously, the number of required communication rounds decreases by roughly an order of magnitude. The per-iteration computational cost increase is  $\sim 20\%$  in our modular implementation.

### B. Generalization Capabilities

This subsection investigates the generalization capabilities of the proposed GCN-WMMSE architecture. The scenario configuration for the training set and the validation set is given in Tab. II unless defined otherwise. We study the relative achievable WSR of GCN-WMMSE networks by varying individual scenario parameters (i) given a network trained on samples with matching scenario configuration to the validation data, denoted by MT, (ii) given a network which is only trained on samples at a defined pivot scenario configuration, denoted by PT, and (iii) given a network which uses a training set containing random scenario configurations, denoted by DT. The achievable WSR of the WMMSE algorithm with MRC initialization is not provided in this section since it is consistently outperformed by WMMSE RI in our experiments.

1) *BS Power and UE Noise Power*: In Fig. 4, we sweep the BS power budget (top left) or UE noise power (top right), while GCN-WMMSE PT is trained with  $P_{\text{BS}} = 30$  dBm or  $\sigma_{\text{UE}}^2 = -100$  dBm, respectively. GCN-WMMSE MT consistently achieves over 93.64% relative WSR, closely following WMMSE RI and outperforming the WMMSE RI TR significantly, especially for high values of  $P_{\text{BS}}$ . GCN-WMMSE PT generalizes well to scenarios with higher BS power compared to scenarios in its training data, however, it sacrifices some relative WSR for lower BS power. In case of a  $-15$  dB offset from the training data, the relative WSR achieved by GCN-WMMSE PT falls below the value of WMMSE RI TR. On the other hand, the achievable WSR for rising SNR remains close to WMMSE RI. For varying noise levels  $\sigma_{\text{UE}}^2$ , both GCN-WMMSE MT and GCN-WMMSE PT consistently outperform WMMSE RI TR, and GCN-WMMSE MT even outperforms WMMSE RI in case of low noise.

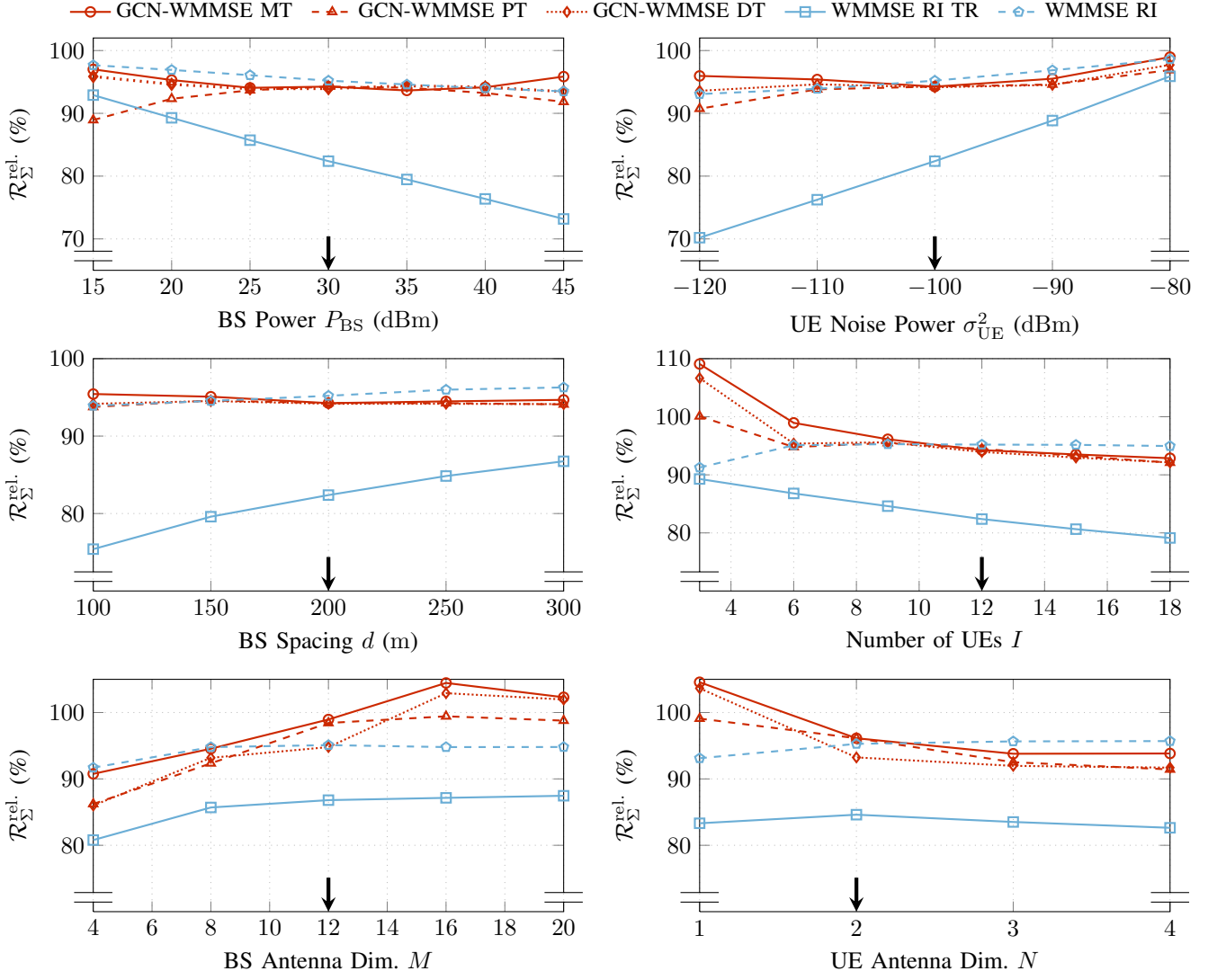


Figure 4. Generalization of GCN-WMMSE (proposed) w.r.t. several wireless scenario parameters. The arrows indicate the configuration for the training of GCN-WMMSE PT networks. Top: BS power budgets  $P_k$  (left) and UE noise power  $\sigma_{\text{UE}}^2$  (right). Middle: BS separation distances  $d_{\text{BS}}$  (left) and number of UEs (right). Bottom: Numbers of antenna elements at the BSs (left) and at the UEs (right).

2) *Network Density*: Fig. 4 (middle left) illustrates the generalization w.r.t. the BS distance  $d_{\text{BS}}$ . GCN-WMMSE PT is trained with  $d_{\text{BS}} = 200$  m. In this case, both the GCN-WMMSE MT and PT networks closely follow the WSR of WMMSE RI, significantly above the truncated algorithm and achieving rates above 93.76% relative to WMMSE50. This can be explained by the signal-to-noise-plus-interference ratio (SINR) at the UEs staying approximately constant if  $d_{\text{BS}}$  changes and the interference is significant.

3) *Array Dimensions*: In Fig. 4 (bottom left), we study a changing BS antenna dimension with  $I = 6$  UEs. GCN-WMMSE PT is trained with  $M = 12$ . GCN-WMMSE MT performs well for  $M < 12$  and substantially outperforms WMMSE RI with 100 iterations for  $M \geq 12$ . In this case, the classical WMMSE algorithm tends to find suboptimal beamformers with significant differences between individual UE rates per scenario realization while the unfolded algorithm favors solutions with uniformly distributed rates. GCN-WMMSE PT outperforms WMMSE RI for  $M \geq 12$  as well, but to a lesser extent.

Varying numbers of UE antenna elements are considered in Fig. 4 (bottom right) with  $I = 9$  UEs. GCN-WMMSE PT and GCN-WMMSE MT outperform WMMSE RI TR, both achieving a rate above 91.43% relative to WMMSE50. For  $N = 1$ , WMMSE RI is substantially outperformed.

These generalization capabilities can be leveraged in training to facilitate training data collection. Instead of sharing the full channel matrices, truncated channels can be collected at a learning node to reduce communication overhead and to decrease the computational cost in online training applications, see Section IV-D.

We remark that both the WMMSE and GCN-WMMSE can experience numerical difficulties when the number of BS antennas  $M$  exceeds the total number of antennas of all UEs. In this case, if the candidate beamformers  $\tilde{\mathbf{V}}_i$  are additionally (almost) orthogonal to the nullspace of  $\mathbf{R}_k$  and it holds that  $\sum_{i \in \mathcal{I}_k} \|\mathbf{R}_k^\top \tilde{\mathbf{V}}_i\|_F^2 \leq P_k$ , the minimization of (2) w.r.t.  $\mathbf{V}$ , a quadratically constrained quadratic program (QCQP) which is solved by the updates (3c) and (3d), becomes ill-conditioned. In literature, this is known as the (near) hard case

of a QCQP [48]. Our results indicate that GCN-WMMSE is more robust than the WMMSE algorithm in wireless scenarios prone to this issue. Additional remedies include replacing the operations (3c) and (3d) with a specialized iterative solver that achieves a higher accuracy in such instances [48]. Note that ill-conditioned instances do not occur if  $K = 1$ .

4) *Number of UEs*: Lastly, Fig. 4 (middle right) shows the achieved relative WSR given a varying number of UEs  $I$ . GCN-WMMSE MT generalizes well, approximately matching or outperforming WMMSE RI on average. GCN-WMMSE PT is trained on data with 12 UEs and generalizes well to lower  $I$ , achieving a  $\mathcal{R}_{\Sigma}^{\text{rel.}}$  of 96.09%. For  $I = 18$  UEs, it outperforms WMMSE RI TR by 13%. It is thus advantageous to train with the maximum number of UEs disregarding the increased complexity of training.

5) *Training on Random Scenario Parameters*: Instead of relying on pure transfer learning, i.e., if training and test data have different statistics, GCN-WMMSE DT leverages datasets containing random scenario parameters. As Fig. 4 demonstrates, this is advantageous in case of the BS power or UE receiver noise, and similar in performance in case of diverse BS distances. For changing antenna dimensions, this training scheme is beneficial compared to GCN-WMMSE PT when the number of BS antennas is high or in the case of single-antenna receivers. Similarly, it outperforms pure transfer learning for a low number of UEs.

### C. DeepMIMO Dataset

The DeepMIMO dataset [47] contains precomputed, ray-traced CSI for an urban scenario. It offers multiple BSs and thousands of possible UEs positions. The dataset enables the evaluation of the proposed GCN-WMMSE architecture for correlated channel coefficients.

Three specific scenario configurations, denoted as DM S1, DM S2 and DM S3 respectively, with dataset parameters as in Tab. IX are defined. Furthermore, we set  $P_{\text{BS}} = 30$  dBm,  $\sigma_{\text{UE}}^2 = -90$  dBm,  $B = 240$  kHz, and consider a single OFDM carrier. The BS antennas are spaced by half a wavelength. For each configuration the set of UE positions is split in two halves which are then assigned to their closest BSs. Afterwards, 5000 random sets of 16 UEs, 3 per BS, are sampled as training data, and 1000 sets are sampled as validation data. The sets of UE positions in training and validation data are disjoint.

We train the GCN-WMMSE networks similarly to the previous experiments with hyperparameters summarized in Tab. I while the number of layers  $L$  is set to 5. As Tab. X shows, the proposed GCN-WMMSE networks achieve at least 89.43% of WMMSE50, outperforming the WMMSE RI TR with  $L = 5$  iterations by at least 10%. It improves over WMMSE RI in DM S1 and DM S2, but falls 4% short in DM S3. In the latter scenario, increasing the number of layers improves the performance. Furthermore, a network model trained on DM S1 generalizes with little performance loss to DM S2. Overall, the benefit of a significantly reduced number of required iterations observed in the Rayleigh fading scenario transfers to the ray-tracing channel model.

### D. Case Study: Finetuning in Dynamic Scenarios

Although GCN-WMMSE exhibits significant generality, finetuning of a network model by learning on current data may still be beneficial in case of changing wireless conditions. Therefore, it is intriguing to leverage the characteristics of GCN-WMMSE to enable efficient finetuning. To verify this idea, we consider two DeepMIMO scenarios S4a and S4b, see Tab. IX. Contrary to S4a, scenario S4b features a number of UEs tightly clustered in a hotspot. A GCN-WMMSE model is then trained on S4a, after which the model is transferred to scenario S4b and finetuned for  $T = 250$  steps. Given local CSI availability, it is of interest to reduce the transfer of channel samples to a training node to a minimum. We thus limit the number of samples available to the finetuning stage to 100 to take advantage of the training data efficiency of GCN-WMMSE. Furthermore, we truncate channel matrices from  $4 \times 12$  to  $3 \times 9$  to leverage generality in the antenna dimension, almost halving the size of the channel data. This additionally reduces the computational cost of training. All other simulation parameters are as in Section IV-C.

Tab. X demonstrates that finetuning with the small truncated dataset can improve the performance by almost 2% over pure model transfer, which approaches the performance of the model trained on S4b. Thus, the properties of GCN-WMMSE enable efficient online training with distributed data collection.

## V. RELATED WORK

In this section, we discuss previous model architectures based on WMMSE algorithm unrolling. We focus on the works [23]–[25] specifically. Tab. XI provides an overview. These works limit the network domain compared to the classical WMMSE, and particularly the architectures considered in [24], [25] cannot easily be extended to the general setup considered in this paper. We thus compare to the proposed GCN-WMMSE on the respective limited scenario setup. If not mentioned otherwise, all networks are trained using the training hyperparameters in Tab. I.

### A. UWMMSE

The authors of [25] introduce the UWMMSE (Unfolded WMMSE) architecture which is limited to transmitter-receiver pairs ( $K = I$ ) and optimization of power allocation on SISO links ( $M = N = 1$ ). The problem reduces to real variables and problem (3c) significantly simplifies. The architecture aims to reduce the number of required iterations compared to the original WMMSE algorithm by transforming the weight scalars  $w_i$  (1-dimensional weight matrix  $\mathbf{W}_i$ ) by an affine mapping. The mapping coefficients are obtained by 2-layer GCNs with a shift matrix consisting of all channels and trainable input vectors. For more details, see [25].

Models based on both the UWMMSE and proposed GCN-WMMSE architecture are compared on SISO scenarios with a similar channel model as in [25, Section 4E]: For each channel sample,  $K$  transmitters are placed randomly at a location  $\mathbf{p}_{\text{Tx},i} \in [-K/d, K/d]^2$  and their paired receiver is placed at random at  $\mathbf{p}_{\text{Tx},i} + \mathbf{o}_{\text{Rx},i}$  where  $\mathbf{o}_{\text{Rx},i} \in [-M/4, M/4]^2$ . Parameter  $d$  denotes the network density. The scalar channel

Table IX  
DEEP MIMO SCENARIO CONFIGURATION USING DATASET ‘O1’.

Scenario Configuration	DM S1	DM S2	DM S3	DM S4a	DM S4b
Active BSs	13, 14, 15, 16	5, 6, 7, 8	6, 8, 17, 18	13, 14, 15, 16	13, 14, 15, 16
Active UE Rows	2752 to 3600	1400 to 1900	3853 to 4750	2752 to 3600	3300 to 3400
Number of active UEs	16	16	16	4	12
Number of BS Antennas	$4 \times 3 \times 1$	$4 \times 3 \times 1$	$4 \times 3 \times 1$	$4 \times 3 \times 1$	$4 \times 3 \times 1$
Number of UE Antennas	1	1	2	4	4

Table X  
RATE AND RELATIVE RATE OF GCN-WMMSE (PROPOSED) COMPARED TO WMMSE50 ON THE DEEP MIMO DATA SET SCENARIOS.

Scenario Configuration	Rel. Rate $\mathcal{R}_{\Sigma}^{\text{rel.}}$ (%)			Abs. Rate $\mathcal{R}_{\Sigma}$ ( $\frac{\text{nat}}{\text{Hz}}$ )
	GCN-WMMSE	WMMSE RI	WMMSE RI TR	WMMSE 50
DM S1	93.47	91.76	78.68	38.61
DM S2	91.60	90.63	75.62	49.63
DM S2 (trained on DM S1)	90.05	90.63	75.62	49.63
DM S3	89.43	93.43	78.45	50.06
DM S4b	90.23			
DM S4b (trained on DM S4a)	86.35	94.21	81.88	35.61
DM S4b (trained on DM S4a, finetuned)	88.29			

Table XI  
OVERVIEW OF A SELECTION OF RELATED ARCHITECTURES.

Acronym	Explanation	Domain
UWMMSE [25]	Integration of GCN.	SISO Tx-Rx-pairs.
PGD WMMSE [23]	PGD with learnable step size.	Extendable to cellular MU-MIMO.
IAIDNN [24]	Trainable 1st-order approximation.	Single-cell MU-MIMO.

is given by  $h_{ij} = |\mathbf{o}_{\text{Rx},i}|^{-2.2} h_{f,ij}$  where  $h_{f,ij}$  is drawn from a Rayleigh distribution with mode 1. The large-scale path loss  $|\mathbf{o}_{\text{Rx},i}|^{-2.2}$  is bounded by 1 from above.

For the following experiments, the number of layers  $L$  of both networks is set to 4. The UWMMSE network uses 2-layered GCNs with a hidden layer dimension of 4, the GCN-WMMSE models adopt  $F$  and  $G$  from Tab. I. First, following [25], both networks are trained on randomly sampled channels with fixed  $M = 20$  transceiver pairs and density drawn from  $[0.5, 5]$  uniformly at random. The networks are validated on a sample set with fixed density  $d$  and 1000 samples each. Fig. 5 (left) shows that both networks outperform the truncated WMMSE with MRC initialization, with the gap increasing for denser and more difficult scenarios. We only show WMMSE MRC since it consistently outperforms WMMSE RI in these scenarios. GCN-WMMSE outperforms the SISO-specific UWMMSE with an exception at density  $d = 5$ , where UWMMSE closely approaches the converged WMMSE. Note that for  $d = 1$ , UWMMSE and GCN-WMMSE achieve a rate of  $50.14 \frac{\text{nat}}{\text{Hz}}$  and  $50.59 \frac{\text{nat}}{\text{Hz}}$ , respectively; the classical WMMSE algorithm only approaches a similar result after 11 or 17 iterations, respectively.

We repeat the experiment with fixed  $d = 1$  and instead vary the number of pairs  $K$  from 5 to 50. As indicated in Fig. 5 (right), GCN-WMMSE outperforms UWMMSE, achieving consistently between 92% to 95% of WMMSE50, ahead of WMMSE MRC TR. In conclusion, the proposed GCN-WMMSE architecture generalizes well to pairwise

SISO scenarios, and outperforms the less general scenario-configuration-specific architecture in most cases. Our results for UWMMSE networks match the results reported in the original work [25]. Recently, the same authors published an extension of UWMMSE for MIMO links [29], however, compared to GCN-WMMSE it is restricted to pairwise links and real channels and parameter sets are unflexible w.r.t. array dimensions.

### B. Unfolded PGD

In [23], single-cell scenarios with single-antenna UEs are exclusively studied. Here, the application of KKT conditions (as in (3c) and (3d)) is avoided by computing the subproblem for  $\mathbf{V}$  using a finite number  $Q$  of sub-iterations of PGD on the WMMSE objective (2) w.r.t.  $\mathbf{V}$ . The PGD step-sizes  $\gamma_{\ell q}$  are chosen as trainable parameters, where  $q = 1, \dots, Q$  is the PGD sub-step index within an outer WMMSE layer  $\ell$ . This particular unfolding can be straightforwardly extended to multicell scenarios, as alluded to by the original authors. Furthermore, we extend the approach to the case where  $N_i > 1$  as opposed to  $N_i = 1$  as considered by the original authors, leading to the subiteration update  $\hat{\mathbf{V}}_i^{(\ell,q)} = \mathbf{V}_i^{(\ell,q-1)} - \gamma_{\ell q} \left( \mathbf{R}_k^{(\ell)} \mathbf{V}_i^{(\ell,q-1)} - \tilde{\mathbf{V}}_i^{(\ell)} \right)$  where  $\mathbf{V}_i^{(\ell,0)} = \mathbf{V}_i^{(\ell-1)}$ . Each substep is succeeded by an Euclidian projection (15) to the feasible set.

We compare the achievable rate obtained by the unfolded PGD WMMSE to the proposed GCN-WMMSE. The GCN-WMMSE networks are trained using the same hyperparameters as in Tab. I, while the unfolded PGD WMMSE is trained for  $T = 20000$  steps with a multiplicative step size decay of 0.1 after 5000 steps each and  $\mathcal{L} = \{1, \dots, L\}$ . All networks are configured for  $L = 7$  layers. In Scenario I, the networks are trained and validated on scenarios with  $K = 4$  BSs with  $M = 4$ , and  $I = 8$  UEs uniformly assigned with  $N = 2$ . Channel matrix coefficients are drawn from  $\mathcal{CN}(0, 1)$  and we set  $\sigma_{\text{UE}}^2 = 0$  dBm and  $P_{\text{BS}} = 20$  dBm.

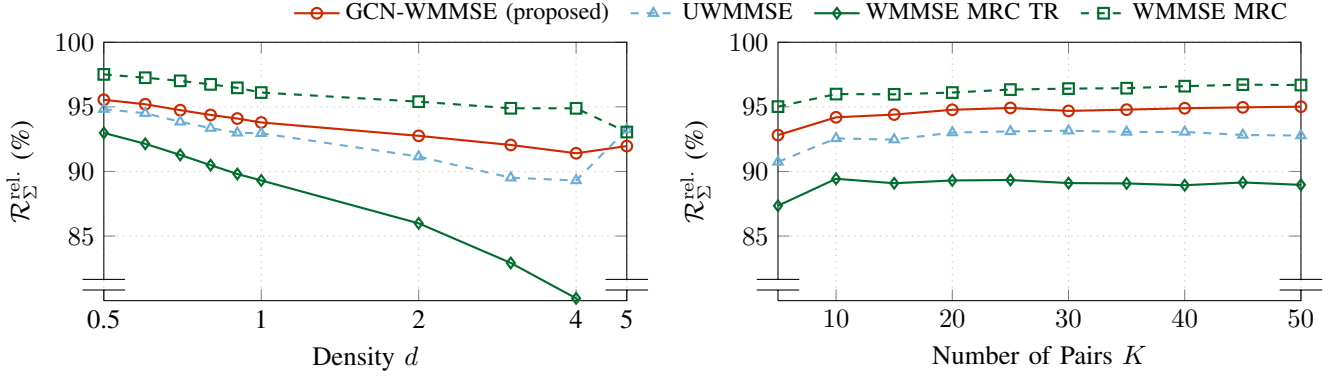


Figure 5. UWMMSE [25] and GCN-WMMSE (proposed) for varying density  $d$  (left) or number of pairs  $K$  (right).  $P_{BS} = 0$  dBm,  $\sigma_{UE}^2 = -92$  dBm.

Table XII  
RELATIVE WSR OF THE UNFOLDED PGD IN MULTICELL MU-MIMO COMPARED TO GCN-WMMSE (PROPOSED).

Scenario	Unfolded PGD $\mathcal{R}_{\Sigma}^{\text{rel.}} (\%)$				GCN-WMMSE $\mathcal{R}_{\Sigma}^{\text{rel.}} (\%)$	WMMSE50 $\mathcal{R}_{\Sigma} (\frac{\text{nat}}{\text{Hz}})$
I: Simple Rayleigh	$Q = 4$	$Q = 8$	$Q = 12$	$Q = 16$	89.21	25.22
	69.71	77.87	80.77	81.84		
II: Scenario of Tab. II	$Q = 16$	$Q = 24$	$Q = 32$	$Q = 40$	94.26	92.56
	46.30	48.88	48.88	52.31		

Tab. XII (Scenario I) demonstrates that the unfolded PGD WMMSE model achieves 81.84% relative WSR with 16 PGD substeps, clearly saturating w.r.t. the number of substeps  $Q$ . In comparison, the proposed GCN-WMMSE achieves 89.21%. We remark, however, that this comes at the cost of an eigendecomposition of  $4 \times 4$  matrices in (6), which significantly contributes to the total computational cost.

On the other hand, when considering scenarios as in section IV-B with parameters as in Tab. II, the unfolded PGD fails to achieve a relative WSR above 53% for  $Q = 40$  subiterations. Higher required values for  $Q$  are expected as  $M$  increases, however, a saturation in performance is evident. This can be attributed to reciprocal interference alignment [41], [49] which leads to the eigenvalues of  $\mathbf{R}_k^{(\ell)}$  becoming more dissimilar with increasing iteration index  $\ell$ , SNR or degrees of freedom of the scenario. A badly conditioned matrix can drastically decrease the convergence speed of a first-order QCQP optimization methods such as PGD [50, Th. 11]. Therefore, globally trained PGD step sizes are too large and do not accurately converge towards the local optimum. In comparison, (3c) and (3d) correspond to a second-order method.

### C. IAIDNN

The authors of [24] consider single-cell MU-MIMO scenarios. In this limited case, the power constraint is guaranteed to be exactly met. Hu et al. consequently construct an equivalent objective to the WSR maximization by absorbing the constraint into the objective function, thereby developing a WMMSE-like algorithm without Lagrangian dual variables and eigendecompositions. Within the architecture based on unrolling this algorithm, that is termed iterative algorithm-induced deep neural network (IAIDNN), matrix inverse multiplications, e.g., for a matrix  $\mathbf{B}_i^{-1} \tilde{\mathbf{V}}_i$ , are approximated by

Table XIII  
PERFORMANCE OF IAIDNN COMPARED TO GCN-WMMSE (PROPOSED) ON SINGLE-CELL SCENARIOS WITH  $P_{BS} = 20$  dBm,  $\sigma^2 = 0$  dBm AND  $N = 2$ . \* INDICATES THE RESULTS REPORTED IN [24].

Scenario ( $M, I$ )		(8, 4)	(16, 8)	(32, 16)
Abs. Rate $\mathcal{R}_{\Sigma} (\frac{\text{nat}}{\text{Hz}})$	WMMSE50	32.22	58.53	112.08
	IAIDNN	85.35	90.52	91.93
Rel. Rate $\mathcal{R}_{\Sigma}^{\text{rel.}} (\%)$	IAIDNN Imp.	82.31	86.49	91.38
	IAIDNN SP	—	87.29	—
	*IAIDNN [24]	*91.35	*92.13	*92.63
	GCN-WMMSE	96.34	101.66	101.65

the operation  $\mathbf{B}_i^{-1} \tilde{\mathbf{V}}_i \approx (\mathbf{B}_i^+ \mathbf{X}_i^b + \mathbf{B}_i \mathbf{Y}_i^b + \mathbf{Z}_i^b) \tilde{\mathbf{V}}_i + \mathbf{O}_i^b$  which is derived from the first-order Taylor approximation of the inverse. The matrix  $\mathbf{B}_i^+$  is the inverse diagonal of  $\mathbf{B}_i$ . Note that the conformable parameter matrices  $\mathbf{X}_i^b$ ,  $\mathbf{Y}_i^b$ ,  $\mathbf{Z}_i^b$  and  $\mathbf{O}_i^b$  are separate for every UE index  $i$ . Furthermore, the V-step in the last layer remains exempt from the approximation, which is empirically critical to achieve a high WSR. The authors set  $\mathbf{Y}_i^b = 0$  for all  $i$  in practice. For more details, see [24]. Although somewhat similar to the proposed GCN-WMMSE architecture on first glance, the GCN-WMMSE network components are motivated by graph filters and feature augmentations such as nonlinearities and skip connections. Additionally, it is fully general with any given parameter set and is suitable for multicell scenarios, while a particular parameter set limits IAIDNN in its number of UEs or number of supported antennas.

We reimplemented the IAIDNN architecture in PyTorch, taking advantage of automatic differentiation and ADAMW optimizers instead of a manual gradient computation as in [24]. The IAIDNN networks are trained with a step size of  $10^{-3}$ , which is decayed after 2500 steps each, beginning at  $t = 5000$ . The IAIDNN hyperparameters are tailored to the scenario configurations while the GCN-WMMSE networks adopt the parameters from Tab. I. The number of network

Table XIV  
AVERAGE UE RATES FOR A MIMO BROADCAST CHANNEL WITH  $M = 16$  AND  $I = 8$  IN  $\frac{\text{nat}}{\text{Hz}}$  FOR WMMSE MRC, IAIDNN AND IAIDNN WITH PARAMETERS SHARED ACROSS UES (IAIDNN SP).

User $i$	Sum	1	2	3	4	5	6	7	8
WMMSE MRC	58.25	7.40	7.38	7.15	7.22	7.23	7.29	7.30	7.28
IAIDNN	52.98	8.14	8.13	8.12	4.06	4.0	4.15	8.14	8.16
IAIDNN SP	51.10	6.39	6.41	6.34	6.38	6.47	6.37	6.33	6.41

layers is  $L = 7$ . Only single-cell scenarios are considered and channel matrix coefficients are sampled from  $\mathcal{CN}(0, 2)$  as in [24].

As Tab. XIII demonstrates, the proposed GCN-WMMSE networks outperform the IAIDNN networks by 9% (compared to results reported in [24]) for  $M = 16$  and 32 with the same number of layers, however, note the computational cost of the eigendecomposition. We were unable to reproduce the results reported in [24] exactly, especially regarding the improved IAIDNN architecture which applies matrix inversions. We further remark that an IAIDNN network produces degenerate asymmetric results on symmetric data sets. Specifically, some UE indices are on average disadvantaged w.r.t. their UE rate  $\mathcal{R}_i$ , as Tab. XIV demonstrates. This can be attributed to using different network parameter groups per UE index  $i$ , leading to some receive signal spaces of some receivers being permanently assigned to interference. Employing shared parameters (SP) instead leads to balanced rates between indices  $i$  while also reducing the number of trainable parameters and reducing the computational complexity. However, the WSR slightly reduces due to slower convergence since interference allocation is not a priori anymore. This proves the importance of ensuring equivariance for machine learning models in such optimization problems.

## VI. CONCLUSION

We propose a distributed unrolled architecture based on the classical WMMSE algorithm, termed GCN-WMMSE, which is applicable to multicell MU-MIMO wireless networks. Although the computation complexity per iteration is of the same order as the original WMMSE algorithm, the number of iterations is massively reduced while achieving a similar rate as the WMMSE, decreasing the communication overhead in a distributed deployment. For the same set of parameters, it maintains its performance across changing scenario configurations in most instances, proving its excellent generalization capabilities. Additionally, it compares favorably to previous unrolled WMMSE architectures despite its generality. Future investigations could address suitable approximate solutions of the downlink beamformer subproblem in multicell MU-MIMO networks. Furthermore, it must be noted that the instantaneous capacity model has practical limitations and the more appropriate ergodic channel model is subject to subsequent research.

## REFERENCES

- [1] R. W. Heath Jr. and A. Lozano, *Foundations of MIMO Communication*. Cambridge University Press, 2018. DOI: 10.1017/9781139049276.
- [2] Z.-Q. Luo and S. Zhang, "Dynamic spectrum management: Complexity and duality," *IEEE Journal of Selected Topics in Signal Processing*, vol. 2, no. 1, pp. 57–73, 2008. DOI: 10.1109/JSTSP.2007.914876.
- [3] R. Hunger, D. Schmidt, and M. Joham, "A combinatorial approach to maximizing the sum rate in the MIMO BC with linear precoding," *2008 42nd Asilomar Conference on Signals, Systems and Computers*, pp. 316–320, 2008.
- [4] E. Björnson, G. Zheng, M. Bengtsson, and B. E. Ottersten, "Robust monotonic optimization framework for multicell MISO systems," *CoRR*, vol. abs/1104.5240, 2011. arXiv: 1104.5240. [Online]. Available: <http://arxiv.org/abs/1104.5240>.
- [5] Q. Shi, M. Razaviyayn, Z. Luo, and C. He, "An iteratively weighted MMSE approach to distributed sum-utility maximization for a MIMO interfering broadcast channel," *IEEE Transactions on Signal Processing*, vol. 59, no. 9, pp. 4331–4340, 2011. DOI: 10.1109/TSP.2011.2147784.
- [6] K. Shen and W. Yu, "Fractional programming for communication systems—part I: Power control and beamforming," *IEEE Transactions on Signal Processing*, vol. 66, no. 10, pp. 2616–2630, 2018. DOI: 10.1109/TSP.2018.2812733.
- [7] E. Peltonen, M. Bennis, M. Capobianco, M. Debbah, A. Y. Ding, F. J. Gil-Castiñeira, M. Jürmu, T. Karvonen, M. Kelanti, A. Kliks, T. Leppänen, L. Lovén, T. Mikkonen, A. Rao, S. Samarakoon, K. Seppänen, P. Sroka, S. Tarkoma, and T. Yang, "6G white paper on edge intelligence," *CoRR*, vol. abs/2004.14850, 2020. arXiv: 2004.14850. [Online]. Available: <https://arxiv.org/abs/2004.14850>.
- [8] E. Björnson, L. Sanguinetti, H. Wymeersch, J. Hoydis, and T. L. Marzetta, *Massive MIMO is a reality – what is next? five promising research directions for antenna arrays*, 2019. arXiv: 1902.07678 [eess.SP].
- [9] S. Zhang and D. Zhu, "Towards artificial intelligence enabled 6G: State of the art, challenges, and opportunities," *Computer Networks*, vol. 183, p. 107556, 2020, ISSN: 1389-1286. DOI: <https://doi.org/10.1016/j.comnet.2020.107556>. [Online]. Available: <https://www.sciencedirect.com/science/article/pii/S138912862031207X>.
- [10] U. Challita, L. Dong, and W. Saad, "Proactive resource management in LTE-U systems: A deep learning perspective," *CoRR*, vol. abs/1702.07031, 2017. arXiv: 1702.07031. [Online]. Available: <http://arxiv.org/abs/1702.07031>.
- [11] N. Samuel, T. Diskin, and A. Wiesel, "Deep MIMO detection," in *2017 IEEE 18th International Workshop on Signal Processing Advances in Wireless Communications (SPAWC)*, 2017, pp. 1–5. DOI: 10.1109/SPAWC.2017.8227772.
- [12] D. Neumann, T. Wiese, and W. Utschick, "Deep channel estimation," in *WSA 2017; 21th International ITG Workshop on Smart Antennas*, 2017, pp. 1–6.
- [13] H. Sun, X. Chen, Q. Shi, M. Hong, X. Fu, and N. D. Sidiropoulos, "Learning to optimize: Training deep neural networks for interference management," *IEEE Transactions on Signal Processing*, vol. 66, no. 20, pp. 5438–5453, 2018. DOI: 10.1109/TSP.2018.2866382.
- [14] A. Alkhateeb, S. Alex, P. Varkey, Y. Li, Q. Qu, and D. Tujkovic, "Deep learning coordinated beamforming for highly-mobile millimeter wave systems," *IEEE Access*, vol. 6, pp. 37 328–37 348, 2018. DOI: 10.1109/ACCESS.2018.2850226.
- [15] M. Eisen and A. Ribeiro, "Optimal wireless resource allocation with random edge graph neural networks," *IEEE Transactions on Signal Processing*, vol. 68, pp. 2977–2991, 2020. DOI: 10.1109/TSP.2020.2988255.
- [16] W. Xia, G. Zheng, Y. Zhu, J. Zhang, J. Wang, and A. P. Petropulu, "A deep learning framework for optimization of MISO downlink beamforming," *IEEE Transactions on Communications*, vol. 68, no. 3, pp. 1866–1880, 2020. DOI: 10.1109/TCOMM.2019.2960361.
- [17] H. Huang, W. Xia, J. Xiong, J. Yang, G. Zheng, and X. Zhu, "Unsupervised learning-based fast beamforming design for downlink MIMO," *IEEE Access*, vol. 7, pp. 7599–7605, 2019. DOI: 10.1109/ACCESS.2018.2887308.
- [18] K. Gregor and Y. LeCun, "Learning fast approximations of sparse coding," in *Proceedings of the 27th International Conference on*



- International Conference on Machine Learning*, ser. ICML'10, Haifa, Israel: Omnipress, 2010, pp. 399–406, ISBN: 9781605589077.
- [19] V. Monga, Y. Li, and Y. C. Eldar, *Algorithm unrolling: Interpretable, efficient deep learning for signal and image processing*, 2020. arXiv: 1912.10557 [eess.IV].
- [20] A. Balatsoukas-Stimming and C. Studer, *Deep unfolding for communications systems: A survey and some new directions*, 2019. arXiv: 1906.05774 [eess.SP].
- [21] M. Zhu, T. Chang, and M. Hong, “Learning to beamform in heterogeneous massive MIMO networks,” *CoRR*, vol. abs/2011.03971, 2020. arXiv: 2011.03971. [Online]. Available: <https://arxiv.org/abs/2011.03971>.
- [22] Y.-F. Liu, Y.-H. Dai, and Z.-Q. Luo, “Coordinated beamforming for MISO interference channel: Complexity analysis and efficient algorithms,” *IEEE Transactions on Signal Processing*, vol. 59, no. 3, pp. 1142–1157, 2011. DOI: 10.1109/TSP.2010.2092772.
- [23] L. Pellaco, M. Bengtsson, and J. Jaldén, “Deep weighted mmse downlink beamforming,” in *ICASSP 2021 - 2021 IEEE International Conference on Acoustics, Speech and Signal Processing (ICASSP)*, 2021, pp. 4915–4919. DOI: 10.1109/ICASSP39728.2021.9414561.
- [24] Q. Hu, Y. Cai, Q. Shi, K. Xu, G. Yu, and Z. Ding, “Iterative algorithm induced deep-unfolding neural networks: Precoding design for multiuser MIMO systems,” *IEEE Transactions on Wireless Communications*, vol. 20, no. 2, pp. 1394–1410, 2021. DOI: 10.1109/TWC.2020.3033334.
- [25] A. Chowdhury, G. Verma, C. Rao, A. Swami, and S. Segarra, *Unfolding WMMSE using graph neural networks for efficient power allocation*, 2021. arXiv: 2009.10812 [eess.SP].
- [26] J. Zhou, G. Cui, Z. Zhang, C. Yang, Z. Liu, and M. Sun, “Graph neural networks: A review of methods and applications,” *CoRR*, vol. abs/1812.08434, 2018. arXiv: 1812.08434. [Online]. Available: <http://arxiv.org/abs/1812.08434>.
- [27] Y. Shen, Y. Shi, J. Zhang, and K. B. Letaief, “Graph neural networks for scalable radio resource management: Architecture design and theoretical analysis,” *IEEE Journal on Selected Areas in Communications*, vol. 39, no. 1, pp. 101–115, 2021. DOI: 10.1109/JSAC.2020.3036965.
- [28] D. Bertsekas, *Nonlinear Programming*. Athena Scientific, 1999.
- [29] A. Chowdhury, G. Verma, C. Rao, A. Swami, and S. Segarra, *ML-aided power allocation for tactical MIMO*, 2021. arXiv: 2109.06992 [cs.IT].
- [30] T. Liu, A. M. Tillmann, Y. Yang, Y. C. Eldar, and M. Pesavento, “Extended successive convex approximation for phase retrieval with dictionary learning,” *IEEE Transactions on Signal Processing*, vol. 70, pp. 6300–6315, 2022. DOI: 10.1109/TSP.2022.3233253.
- [31] F. Gama, J. Bruna, and A. Ribeiro, “Stability properties of graph neural networks,” *CoRR*, vol. abs/1905.04497, 2019. arXiv: 1905.04497. [Online]. Available: <http://arxiv.org/abs/1905.04497>.
- [32] D. I. Shuman, S. K. Narang, P. Frossard, A. Ortega, and P. Vandergheynst, “The emerging field of signal processing on graphs: Extending high-dimensional data analysis to networks and other irregular domains,” *IEEE Signal Processing Magazine*, vol. 30, no. 3, pp. 83–98, 2013. DOI: 10.1109/MSP.2012.2235192.
- [33] F. Gama, A. G. Marques, G. Leus, and A. Ribeiro, “Convolutional neural network architectures for signals supported on graphs,” *IEEE Transactions on Signal Processing*, vol. 67, no. 4, pp. 1034–1049, 2019. DOI: 10.1109/TSP.2018.2887403.
- [34] I. Loshchilov and F. Hutter, “Fixing weight decay regularization in adam,” *CoRR*, vol. abs/1711.05101, 2017. arXiv: 1711.05101. [Online]. Available: <http://arxiv.org/abs/1711.05101>.
- [35] C. Trabelsi, O. Bilaniuk, D. Serdyuk, S. Subramanian, J. F. Santos, S. Mehri, N. Rostamzadeh, Y. Bengio, and C. J. Pal, “Deep complex networks,” *CoRR*, vol. abs/1705.09792, 2017. arXiv: 1705.09792. [Online]. Available: <http://arxiv.org/abs/1705.09792>.
- [36] F. Wu, A. Souza, T. Zhang, C. Fifty, T. Yu, and K. Weinberger, “Simplifying graph convolutional networks,” in *Proceedings of the 36th International Conference on Machine Learning*, PMLR, 2019, pp. 6861–6871.
- [37] K. He, X. Zhang, S. Ren, and J. Sun, “Deep residual learning for image recognition,” *CoRR*, vol. abs/1512.03385, 2015. arXiv: 1512.03385. [Online]. Available: <http://arxiv.org/abs/1512.03385>.
- [38] R. K. Srivastava, K. Greff, and J. Schmidhuber, “Highway networks,” *CoRR*, vol. abs/1505.00387, 2015. arXiv: 1505.00387. [Online]. Available: <http://arxiv.org/abs/1505.00387>.
- [39] A. Rahimi, T. Cohn, and T. Baldwin, “Semi-supervised user geolocation via graph convolutional networks,” in *Proceedings of the 56th Annual Meeting of the Association for Computational Linguistics (Volume 1: Long Papers)*, Melbourne, Australia: Association for Computational Linguistics, Jul. 2018, pp. 2009–2019. DOI: 10.18653/v1/P18-1187. [Online]. Available: <https://aclanthology.org/P18-1187>.
- [40] H. Amann and J. Escher, *Analysis II*, ser. Grundlehrbuch Mathematik. Birkhäuser Basel, 2008, ISBN: 9783764371050. [Online]. Available: <https://books.google.de/books?id=izgYzhnyacIC>.
- [41] D. A. Schmidt, C. Shi, R. A. Berry, M. L. Honig, and W. Utschick, “Minimum mean squared error interference alignment,” in *2009 Conference Record of the Forty-Third Asilomar Conference on Signals, Systems and Computers*, 2009, pp. 1106–1110. DOI: 10.1109/ACSSC.2009.5470055.
- [42] K. S. Gomadam, V. R. Cadambe, and S. A. Jafar, “Approaching the capacity of wireless networks through distributed interference alignment,” *CoRR*, vol. abs/0803.3816, 2008. arXiv: 0803.3816. [Online]. Available: <http://arxiv.org/abs/0803.3816>.
- [43] S. W. Peters and R. W. Heath, “Cooperative Algorithms for MIMO Interference Channels,” *IEEE Transactions on Vehicular Technology*, vol. 60, no. 1, pp. 206–218, Jan. 2011, ISSN: 0018-9545. DOI: 10.1109/TVT.2010.2085459.
- [44] A. Paszke, S. Gross, F. Massa, A. Lerer, J. Bradbury, G. Chanan, T. Killeen, Z. Lin, N. Gimelshein, L. Antiga, A. Desmaison, A. Kopf, E. Yang, Z. DeVito, M. Raison, A. Tejani, S. Chilamkurthy, B. Steiner, L. Fang, J. Bai, and S. Chintala, “PyTorch: An imperative style, high-performance deep learning library,” in *Advances in Neural Information Processing Systems 32*, H. Wallach, H. Larochelle, A. Beygelzimer, F. d’Alché-Buc, E. Fox, and R. Garnett, Eds., Curran Associates, Inc., 2019, pp. 8024–8035.
- [45] R. Brandt, E. Björnson, and M. Bengtsson, “Weighted sum rate optimization for multicell MIMO systems with hardware-impaired transceivers,” in *2014 IEEE International Conference on Acoustics, Speech and Signal Processing (ICASSP)*, 2014, pp. 479–483. DOI: 10.1109/ICASSP.2014.6853642.
- [46] D. Lopez-Perez, I. Guvenc, and X. Chu, “Mobility management challenges in 3GPP heterogeneous networks,” *IEEE Communications Magazine*, vol. 50, no. 12, pp. 70–78, 2012. DOI: 10.1109/MCOM.2012.6384454.
- [47] A. Alkhateeb, “DeepMIMO: A generic deep learning dataset for millimeter wave and massive MIMO applications,” in *Proc. of Information Theory and Applications Workshop (ITA)*, San Diego, CA, Feb. 2019, pp. 1–8.
- [48] M. Rojas, S. A. Santos, and D. C. Sorensen, “A New Matrix-Free Algorithm for the Large-Scale Trust-Region Subproblem,” *SIAM Journal on Optimization*, vol. 11, no. 3, pp. 611–646, Jan. 2001, ISSN: 1052-6234, 1095-7189. DOI: 10.1137/S105262349928887X.
- [49] K. Gomadam, V. R. Cadambe, and S. A. Jafar, “Approaching the capacity of wireless networks through distributed interference alignment,” in *IEEE GLOBECOM 2008 - 2008 IEEE Global Telecommunications Conference*, 2008, pp. 1–6. DOI: 10.1109/GLOCOM.2008.ECP817.
- [50] I. Necoara, Y. Nesterov, and F. Glineur, *Linear convergence of first order methods for non-strongly convex optimization*, 2016. arXiv: 1504.06298 [math.OC].